
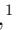













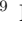
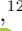


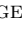




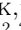
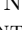
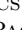
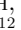



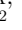
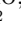





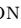

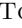



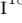


Enhancing Exoplanet Ephemerides by Leveraging Professional and Citizen Science Data: A Test Case with WASP-77A b

FEDERICO R. NOGUER ¹, SUBER CORLEY ¹, KYLE A. PEARSON ², ROBERT T. ZELLEM ²,
MOLLY N. SIMON ¹, JENNIFER A. BURT ², ISABELA HUCKABEE ^{1,2}, PRUNE C. AUGUST ³,
MEGAN WEINER MANSFIELD ^{4,5}, PAUL A. DALBA ^{6,7}, PETER C. B. SMITH ⁸, TIMOTHY BANKS ^{9,10,11},
IRA BELL ^{1,9}, DOMINIQUE DANIEL ¹², LINDSAY DAWSON ^{13,9}, JESÚS DE MULA ⁹, MARC DELDEM ¹²,
DIMITRIOS DELIGEORGOPOULOS ¹², ROMINA P. DI SISTO ^{14,15}, ROGER DYMCK ¹⁶, PHIL EVANS ¹⁷,
GIULIO FOLLERO ¹⁸, MARTIN J. F. FOWLER ¹⁹, EDUARDO FERNÁNDEZ-LAJÚS ¹⁵, ALEX HAMRICK ²⁰,
NICOLETTA IANNASCOLI ¹⁸, ANDRE O. KOVACS ^{21,9}, DENIS HENRIQUE KULH ²², CLAUDIO LOPRESTI ^{12,23,24},
ANTONIO MARINO ¹⁸, BRYAN E. MARTIN ^{25,21}, PAOLO ARCANGELO MATASSA ¹², TASSO AUGUSTO NAPOLEÃO ²²,
ALESSANDRO NASTASI ^{26,27}, ANTHONY NORRIS ⁹, ALESSANDRO ODASSO ¹², NIKOLAOS I. PASCHALIS ^{28,12},
PAVEL PINTR ^{29,12}, JAKE POSTIGLIONE ⁹, JUSTUS RANDOLPH ⁹, FRANÇOIS REGEMBAL ¹², LIONEL ROUSSELOT ¹²,
SERGIO JOSÉ GONÇALVES DA SILVA ²², ANDREW SMITH ⁹ AND ANDREA TOMACELLI ¹⁸

¹*School of Earth and Space Exploration, Arizona State University, 781 E Terrace Mall, Tempe, AZ 85287-6004, United States*

²*Jet Propulsion Laboratory California Institute of Technology, 4800 Oak Grove Drive, Pasadena, CA 91109, USA*

³*DTU Space, Technical University of Denmark, Elektrovej 328, DK-2800 Kgs. Lyngby, Denmark*

⁴*Steward Observatory, University of Arizona, Tucson, AZ 85719, USA*

⁵*NHFP Sagan Fellow*

⁶*Department of Astronomy and Astrophysics, University of California, Santa Cruz, CA 95064, USA*

⁷*SETI Institute, Carl Sagan Center, 339 Bernardo Ave, Suite 200, Mountain View, CA 94043, USA*

⁸*School of Earth & Space Exploration, Arizona State University, Tempe AZ 85287, USA*

⁹*Exoplanet Watch Citizen Scientist Contributor, <https://exoplanets.nasa.gov/exoplanet-watch>*

¹⁰*Dept. of Physical Sci. & Engineering, Harper College, 1200 W Algonquin Rd, Palatine, IL 60067, USA*

¹¹*Nielsen, 675 6th Ave, New York 10011, USA*

¹²*ExoClock Project Citizen Scientist Contributor, <https://www.exoclock.space>*

¹³*Thomas More University, 333 Thomas More Parkway, Crestview Hills, Kentucky*

¹⁴*Facultad de Ciencias Astronómicas y Geofísicas Universidad Nacional de La Plata, Argentina*

¹⁵*Instituto de Astrofísica de La Plata, Observatorio Astronómico de La Plata: Paseo del Bosque, B1900FWA, La Plata, Argentina*

¹⁶*British Astronomical Association*

¹⁷*El Sauce Observatory, Coquimbo Province, Chile*

¹⁸*Unione Astrofili Napoletani, c/o INAF-Osservatorio Astronomico di Capodimonte Napoli via Moiariello, 16 80131 Napoli*

¹⁹*Les Rocquettes Observatory and Exoplanet Factory, South Wonston, Hampshire, SO21 3EX, United Kingdom*

²⁰*Stanford Online High School, 415 Broadway Academy Hall, Floor 2, 8853, Redwood City, CA 94063*

²¹*AAVSO, 185 Alewife Brook Parkway, Suite 410, Cambridge, MA 02138, USA*

²²*Alfa Crucis*

²³*Gruppo Astronomia Digitale (GAD, Italy)*

²⁴*Sezione Pianeti Extrasolari (UAI, Italy)*

²⁵*Tiger Butte Observatory, 2013 Whispering Ridge Dr, Great Falls, MT 59405.*

²⁶*GAL Hassin - Centro Internazionale per le Scienze Astronomiche, Via della Fontana Mitri 3, 90010 Isnello, Palermo, Italy*

²⁷*INAF - Osservatorio Astronomico di Palermo, Piazza del Parlamento, 1, 90134 Palermo, Italy*

²⁸*Nunki Observatory, Skiathos Island, Greece*

²⁹*Institute of Plasma Physics ASCR, v. v. i. Centre TOPTEC, Sobotceka 1660 511 01 Turnov Czech Republic*

1. ABSTRACT

We present an updated ephemeris, and physical parameters, for the exoplanet WASP-77 A b. In this effort, we combine 64 ground- and space-based transit observations, 6 space-based eclipse observations,

and 32 radial velocity observations to produce this target’s most precise orbital solution to date aiding in the planning of James Webb Space Telescope (JWST) and Ariel observations and atmospheric studies. We report a new orbital period of $1.360029395 \pm 5.7 \times 10^{-8}$ days, a new mid-transit time of $2459957.337860 \pm 4.3 \times 10^{-5}$ BJD_{TDB} (Barycentric Julian Date in the Barycentric Dynamical Time scale; Eastman et al. (2010)) and a new mid-eclipse time of $2459956.658192 \pm 6.7 \times 10^{-5}$ BJD_{TDB}. Furthermore, the methods presented in this study reduce the uncertainties in the planet’s mass $1.6654 \pm 4.5 \times 10^{-3} M_{Jup}$ and orbital period $1.360029395 \pm 5.7 \times 10^{-8}$ days by factors of 15.1 and 10.9, respectively. Through a joint fit analysis comparison of transit data taken by space-based and citizen science-led initiatives, our study demonstrates the power of including data collected by citizen scientists compared to a fit of the space-based data alone. Additionally, by including a vast array of citizen science data from ExoClock, Exoplanet Transit Database (ETD), and Exoplanet Watch, we can increase our observational baseline and thus acquire better constraints on the forward propagation of our ephemeris than what is achievable with TESS data alone.

2. INTRODUCTION

Correctly determining a planet’s transit ephemeris is essential for the efficient scheduling of follow-up observations (Zellem et al. 2020) with telescopes such as the James Webb Space Telescope (JWST), the Hubble Space Telescope (HST), or the upcoming Ariel mission scheduled to launch in 2029 that will observe the atmospheres of 1000 exoplanets. Accurate ephemerides help ensure that these highly competitive space-based telescopes are utilized as efficiently as possible to maximize their science output by helping to reduce overheads. Precise exoplanet mid-transit times, whereby a planet passes directly in front of its host star, are crucial for characterizing an exoplanet’s atmosphere through transmission spectroscopy. Due to ephemeris uncertainties, observation time buffers must be included before and after the predicted mid-transit time to ensure that the entire transit is captured in addition to pre and post transit baseline measurements of just the host star flux. As a planet completes additional orbits around its host star, uncertainties in its mid-transit time increase, creating the need for repeated follow-up observations and new analyses (Dragomir et al. 2019; Zellem et al. 2020; Kokori et al. 2023). Since the number of confirmed exoplanets and exoplanet candidates continues to increase, expected to surpass 10,000 from NASA’s TESS mission alone (Kunimoto et al. 2022), there will be a high demand for updated exoplanet ephemerides to enable more efficient analyses of these new worlds.

Previous studies have demonstrated that successfully updating an exoplanet’s mid-transit time can be achieved through collaborations with professionals and citizen scientists utilizing small, ground-based telescopes (see, e.g., Mizrachi et al. 2021; Fowler et al. 2021; Pearson et al. 2022; Hewitt et al. 2023). In one such example, students enrolled in a fully online research course at Arizona State University acquired observations of the planet WASP-104 b taken with a ground-based, robotic, 6-inch telescope (Hewitt et al. 2023; Hewitt et al. 2023b). These students were able to improve upon the uncertainty on the mid-transit time for this particular target by 2.7 percent when compared to the next most recent publication. Efforts like these lay the foundation for continued professional and citizen science-based collaborations that can assist with exoplanet ephemeris maintenance.

Along with a planet’s mid-transit time, the mid-eclipse time is also a crucial parameter for astronomers characterizing exoplanetary atmospheres. During eclipse, the planet passes behind the star, temporarily blocking its reflected light and thermal emission. Eclipses, when the planet passes behind its host star, enable astronomers to measure a planet’s reflected light and thermal emission. For example Smith et al. (2024) leveraged this method with JWST to use the difference in the observed light curve of WASP-77 A b during eclipse, as compared to just before or after, to isolate the planet’s own emission from that of the star. Determining a planet’s mid-eclipse time when an eclipse was not previously observed, requires not only its mid-transit time, but also knowledge of the planet’s eccentricity and argument of periastron, parameters that can be deduced from radial velocity measurements. As such, the inclusion of radial velocity data to the analysis significantly improves precision in predicting transit, eclipse timing (Pearson et al. 2022), and the planet’s orbit for the planning of JWST and Ariel observations (Zellem et al. 2020; Burt et al. 2024, in prep). Additionally, constraints on the planet’s mass helps alleviate degeneracies when performing atmospheric fits (Batalha et al. 2018).

In this effort, we use WASP-77 A b to demonstrate the power of combining a broad suite of transit and eclipse photometry data (collected by both citizen scientists and space-based telescopes) with archival radial velocity data to acquire precise orbital and planetary parameters. WASP-77 A b, a hot Jupiter orbiting a G8 V spectral-type star with $V\text{-mag} = 10.294 \pm 0.007$ (Maxted et al. 2013).

WASP-77 A b has been the target of multiple spectroscopic campaigns designed to measure its atmospheric composition and constrain its formation history. Via high resolution spectroscopic measurements with Gemini-South/IGRINS, WASP-77 A b’s atmosphere was initially inferred to have a subsolar metallicity and solar C/O ratio (Line et al. 2021), an uncommon but not implausible prediction within the core accretion paradigm (e.g., Madhusudhan et al. 2017). Measurements with HST’s Wide Field Camera 3 (WFC3) favored instead a supersolar metallicity (Mansfield et al. 2022), in apparent tension with the previous subsolar inference from Gemini/IGRINS. However, recent observations with JWST/NIRSpec (August et al. 2023) as well as a joint analysis of both the NIRSpec and IGRINS data (Smith et al. 2024), have confirmed the original subsolar metallicity measurement. Additionally, a recent reanalysis of the WFC3 data that takes into account contamination of the stellar companion WASP-77 B found that the WFC3 data indeed also favors a subsolar metallicity (Edwards & Changeat 2024). Within the context of the formation simulations by Bitsch et al. (2022); Khorshid et al. (2023), WASP-77 A b’s atmospheric composition is consistent with formation beyond the CO₂ ice line and inward migration after disk dissipation. The planet star system does not reveal evidence of rapid orbital decay nor other significant orbital perturbations (Cortés-Zuleta et al. 2020). Currently, no additional planetary companions have been reported for WASP 77 A and upper mass limits for potential companions have been calculated by Cortés-Zuleta et al. (2020).

WASP-77 A b is an ideal candidate for this study due the significant amount of archival transit and radial velocity data readily available for this target. As such, to perform the combined transit and radial velocity analysis described in the remainder of this paper, we collected 34 transit photometry data from three different citizen science initiatives: ExoClock (Kokori et al. 2022a,b, 2023), Exoplanet Watch (Zellem et al. 2020), and the Exoplanet Transit Database (ETD)(Poddaný et al. 2010) along with space-based photometry data from two sectors of TESS (Ricker et al. 2015). These mid-transit measurements were combined with archival radial velocity data from the CORALIE and High Accuracy Radial velocity Planet Searcher (HARPS) spectrographs in conjunction with mid-eclipse times derived from JWST, Spitzer and HST. The analysis and methods implemented in this work for WASP-77 A b can be applied when updating the ephemerides of other exoplanets that are high priority targets (e.g., Zellem et al. 2017; Kempton et al. 2018; Hord et al. 2023) for follow-up analysis with larger ground-based or space-based initiatives.

3. OBSERVATIONS

3.1. Citizen Science Data

We incorporated 34 observations from citizen science initiatives (11 from Exoplanet Watch, Table 1; 19 from ExoClock, Table 2; 4 from the Exoplanet Transit Database, Table 3) taken with telescopes as small as 4.5-inch Unistellar (Peluso et al. 2023) eVscopes and the Harvard Smithsonian Center for Astrophysics’ 6-inch “Cecilia” MicroObservatory Robotic Telescope on Mount Hopkins in Arizona (Sadler et al. 2001). Citizen science networks can help refresh and improve transit ephemerides at far less cost than the equivalent effort of larger and more competitive professionally operated facilities (Zellem et al. 2020). For example, the Exoclock project (Kokori 2021; Kokori et al. 2022a,b, 2023) has updated the ephemerides for at least 450 planets using space-based, large ground-based and citizen-science observations from the Exoclock network. The data obtained by citizen scientists is made publicly available to the scientific community. Exoplanet Watch citizen science observations are uploaded to AAVSO and can also be accessed through the Exoplanet Watch website or programmatically with EXOTIC code. Exoclock and ETD also have depositories for their citizen transit data that can be publicly accessed. Figure 1 displays the resulting light curves from all 34 citizen science transit observations.

Table 1. WASP-77 A b Derived Parameters from Exoplanet Watch Transit Data Individual Fits

Observer	Rp/Rs	Mid-transit (BJDTDB)	Inclination (deg.)	σ_{res}
Martin J. F. Fowler (FMAA) (this study)	0.138488 ± 0.011202	2459146.757993 ± 0.003096	85.313903 ± 1.445707	0.011491
Martin J. F. Fowler (FMAA) (this study)	0.130407 ± 0.008210	2459150.837953 ± 0.001785	84.937192 ± 1.059638	0.006623
BTSB (this study)	0.167188 ± 0.009166	2459475.883336 ± 0.002862	89.775798 ± 1.057500	0.010702
Andre O. Kovacs (KADB) (this study)	0.109212 ± 0.002484	2459524.851427 ± 0.000618	89.970091 ± 0.490967	0.008491
Andre O. Kovacs (KADB) (this study)	0.109670 ± 0.003064	2459546.613122 ± 0.000767	89.863576 ± 0.606149	0.007160
Andre O. Kovacs (KADB) (this study)	0.133428 ± 0.004877	2459565.643618 ± 0.001494	87.404846 ± 1.337892	0.009443
Andre O. Kovacs (KADB) (this study)	0.145692 ± 0.001675	2459584.691209 ± 0.000363	84.910237 ± 0.022267	0.006784
Jake Postiglione (PJAE) (this study)	0.140661 ± 0.005349	2459909.739026 ± 0.001112	87.120092 ± 1.155684	0.009801
SAJB (this study)	0.133104 ± 0.000757	2459957.337524 ± 0.000198	88.615123 ± 0.497671	0.003242
Justus Randolph (this study)	0.114845 ± 0.004284	2459845.810377 ± 0.001304	89.984181 ± 0.762004	0.006574
Justus Randolph (this study)	0.121547 ± 0.003251	2459901.578087 ± 0.001122	89.053012 ± 1.047644	0.004139

NOTE—The observations in this table were acquired from NASA Exoplanet Watch citizen science project (Zellem et al. 2020)

Table 2. WASP-77 A b Derived Parameters from ExoClock Transit Data Individual Fits

Observer	Rp/Rs	Mid-transit (BJD)	Inclination (deg.)	σ_{res}
Pavel Pintr (this study)	0.100245 ± 0.003589	2458850.274405 ± 0.000707	88.273883 ± 0.907354	0.001845
Yves Jongen (this study)	0.129250 ± 0.001734	2459067.879321 ± 0.000514	89.150409 ± 0.641214	0.001676
Lorenzo Betti (this study)	0.129802 ± 0.001138	2458431.383446 ± 0.000269	87.606257 ± 0.405009	0.001453
Yves Jongen (this study)	0.124696 ± 0.002344	2459131.799264 ± 0.000654	89.448679 ± 0.781300	0.002639
Paolo Arcangelo Matassa (this study)	0.132062 ± 0.003724	2459568.375690 ± 0.002321	84.917774 ± 1.421284	0.007001
Martin Valentine Crow (this study)	0.140826 ± 0.007180	2459149.479783 ± 0.001457	85.368562 ± 1.203334	0.014618
Alessandro Nastasi (this study)	0.115978 ± 0.002669	2458820.353259 ± 0.000452	89.886516 ± 0.457542	0.003295
Alessandro Nastasi (this study)	0.112150 ± 0.003711	2458790.433805 ± 0.000826	87.571683 ± 1.030419	0.003678
François Regembal (this study)	0.128294 ± 0.003477	2459153.562620 ± 0.000698	87.453267 ± 0.964544	0.005479
Martin Fowler (this study)	0.116704 ± 0.006113	2458855.715261 ± 0.001465	89.997814 ± 1.132437	0.005860
Marc Deldem (this study)	0.122177 ± 0.004267	2457702.409628 ± 0.001268	89.991455 ± 0.845319	0.005132
Yves Jongen (this study)	0.131871 ± 0.002423	2459456.847265 ± 0.000472	87.687640 ± 0.792568	0.002031
Antonio Marino (this study)	0.150334 ± 0.007487	2457377.366686 ± 0.001927	87.237357 ± 1.361995	0.014233
Yves Jongen (this study)	0.130505 ± 0.003079	2459138.600169 ± 0.000722	89.893542 ± 0.743697	0.003175
Dimitrios Deligeorgopoulos (this study)	0.115777 ± 0.003506	2458835.313724 ± 0.000657	87.954140 ± 0.924682	0.004149
Dominique Daniel (this study)	0.127054 ± 0.007057	2459523.492783 ± 0.001510	84.981891 ± 1.009943	0.006525
Claudio Lopresti (this study)	0.129025 ± 0.002699	2459160.361783 ± 0.000740	86.890974 ± 0.908180	0.002571
Nikolaos I. Paschalis (this study)	0.135951 ± 0.006095	2459145.399718 ± 0.001569	89.758226 ± 1.279541	0.009116
Lionel Rousselot (this study)	0.119026 ± 0.004222	2458529.309950 ± 0.000921	89.810029 ± 0.746735	0.003881

NOTE—The observations in this table were acquired from the ExoClock citizen science project (Kokori et al. 2022a,b, 2023)

Table 3. WASP-77 A b Derived Parameters from the Exoplanet Transit Database (ETD) Transit Data Individual Fits

Observer	Rp/Rs	Mid-transit (BJDTDB)	Inclination (deg.)	σ_{res}
Napoleao T., Silva,S., Kulh,D. (this study)	0.125011 ± 0.002695	2458349.782454 ± 0.000589	87.631431 ± 0.892017	0.003467
Phil,Evans (this study)	0.112988 ± 0.000419	2457695.608264 ± 0.000147	89.978600 ± 0.109655	0.005567
Fernández-Lajús E., Di Sisto R. P. (this study)	0.069934 ± 0.001692	2459550.688000 ± 0.000443	85.250493 ± 0.222586	0.001769
Coline Guyot, Julien Dibon (this study)	0.119733 ± 0.001505	2456958.477899 ± 0.000568	84.910753 ± 0.043606	0.005393

NOTE—Observations in this table were acquired from the Exoplanet Transit Database (ETD) (Poddaný et al. 2010)

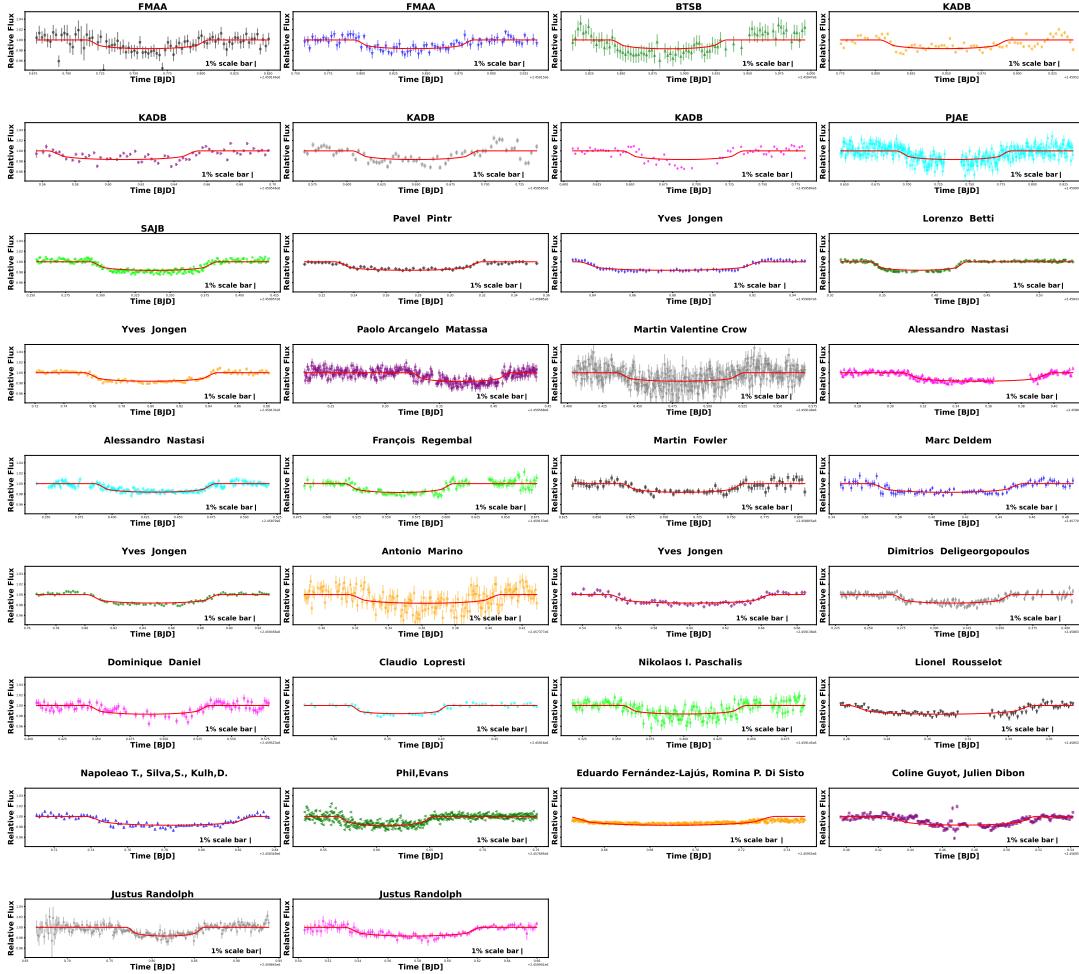


Figure 1. Individual light curves were produced from 34 sets of terrestrial citizen science data during the process described in [Transit Photometry Reduction](#) Section 4.1. Citizen science observations span approximately 8 years from October, 2014 to January, 2023.

3.2. *Transiting Exoplanet Survey Satellite (TESS) Data*

WASP-77 A was observed by TESS during Sector 4 (2018-10-19 to 2018-11-14) and Sector 31 (2020-10-22 to 2020-11-18) in 2 minute cadence during which time WASP-77 A b completed 30 transits (Table 4). The individual time series files used in this study were obtained from public TESS data on the Mikulski Archive for Space Telescopes (MAST) following the prescription described in [Pearson \(2019\)](#), which performs an updated aperture selection and can improve the photometric scatter by up to 30% for some targets by reducing pointing-induced systematics. We removed any data points taken within 30 minutes of the TESS momentum dumps, as these data points typically contain large systematic errors. We next removed 3 sigma outliers from a rolling median filter with a bin size of 32 minutes, as well as any quality-flagged data points. We also applied the Python package WOTAN ([Hippke et al. 2019](#)) to detrend WASP-77 A’s variability from the light curves while ensuring the transit signal remains intact. Figure 2 displays the resulting light curves.

Table 4. WASP-77 A b Derived Parameters from the Transiting Exoplanet Survey Satellite (TESS) Transit Data Individual Fits

Source	Rp/Rs	Mid-transit (BJDTDB)	Inclination (deg.)	σ_{res}
TESS (this study)	0.117211 ± 0.000484	2459169.880555 ± 0.000141	88.173852 ± 0.290894	0.001788
TESS (this study)	0.118047 ± 0.001131	2458416.424934 ± 0.000362	87.712535 ± 0.633352	0.000714
TESS (this study)	0.117444 ± 0.001152	2458428.664764 ± 0.000363	87.963218 ± 0.692152	0.000741
TESS (this study)	0.117935 ± 0.000484	2459145.400138 ± 0.000142	88.168883 ± 0.277498	0.001665
TESS (this study)	0.117839 ± 0.001126	2458430.025059 ± 0.000353	87.884216 ± 0.671382	0.000796
TESS (this study)	0.117399 ± 0.000466	2459164.440698 ± 0.000142	88.106095 ± 0.259252	0.001814
TESS (this study)	0.118875 ± 0.001119	2458415.064802 ± 0.000346	87.598829 ± 0.530363	0.000812
TESS (this study)	0.116758 ± 0.001099	2458435.465274 ± 0.000339	88.042295 ± 0.664903	0.000765
TESS (this study)	0.117346 ± 0.001158	2458412.344649 ± 0.000349	88.291218 ± 0.677087	0.000905
TESS (this study)	0.117514 ± 0.000461	2459150.840086 ± 0.000140	87.934221 ± 0.220790	0.001703
TESS (this study)	0.117219 ± 0.000466	2459160.360695 ± 0.000145	87.852512 ± 0.218656	0.001622
TESS (this study)	0.118470 ± 0.001079	2458431.384909 ± 0.000333	87.716047 ± 0.584771	0.000796
TESS (this study)	0.117228 ± 0.000466	2459146.760236 ± 0.000141	88.069922 ± 0.253357	0.001665
TESS (this study)	0.118145 ± 0.000446	2459154.920533 ± 0.000139	87.800839 ± 0.207198	0.001666
TESS (this study)	0.117360 ± 0.001118	2458417.784887 ± 0.000360	87.782367 ± 0.646523	0.000781
TESS (this study)	0.118147 ± 0.000438	2459161.720527 ± 0.000139	87.843743 ± 0.211657	0.001676
TESS (this study)	0.115917 ± 0.000477	2459167.160783 ± 0.000151	88.613443 ± 0.409135	0.001725
TESS (this study)	0.116917 ± 0.001061	2458427.305095 ± 0.000358	88.297732 ± 0.686959	0.000794
TESS (this study)	0.117727 ± 0.001095	2458413.705108 ± 0.000354	87.799733 ± 0.634761	0.000708
TESS (this study)	0.117967 ± 0.000487	2459163.080668 ± 0.000148	88.139851 ± 0.278206	0.001715
TESS (this study)	0.118133 ± 0.000464	2459153.560254 ± 0.000142	88.156333 ± 0.274597	0.001642
TESS (this study)	0.118279 ± 0.000463	2459168.520838 ± 0.000139	87.931649 ± 0.222379	0.001666
TESS (this study)	0.116907 ± 0.001010	2458425.945066 ± 0.000330	88.750602 ± 0.613404	0.000774
TESS (this study)	0.116926 ± 0.000475	2459148.120307 ± 0.000140	87.840918 ± 0.200418	0.001633
TESS (this study)	0.118292 ± 0.001041	2458434.105215 ± 0.000335	88.173898 ± 0.681437	0.000770
TESS (this study)	0.117624 ± 0.001107	2458432.745412 ± 0.000348	88.002729 ± 0.679718	0.000785
TESS (this study)	0.117233 ± 0.000454	2459152.200533 ± 0.000154	88.415422 ± 0.412857	0.001749
TESS (this study)	0.117431 ± 0.000480	2459165.800856 ± 0.000153	88.291654 ± 0.336392	0.001731
TESS (this study)	0.117304 ± 0.000444	2459159.000638 ± 0.000143	88.147033 ± 0.260625	0.001661
TESS (this study)	0.116017 ± 0.000440	2459149.480297 ± 0.000159	88.157882 ± 0.301488	0.001661

NOTE—TESS observations in this table were acquired from the Mikulski Archive for Space Telescopes (MAST).

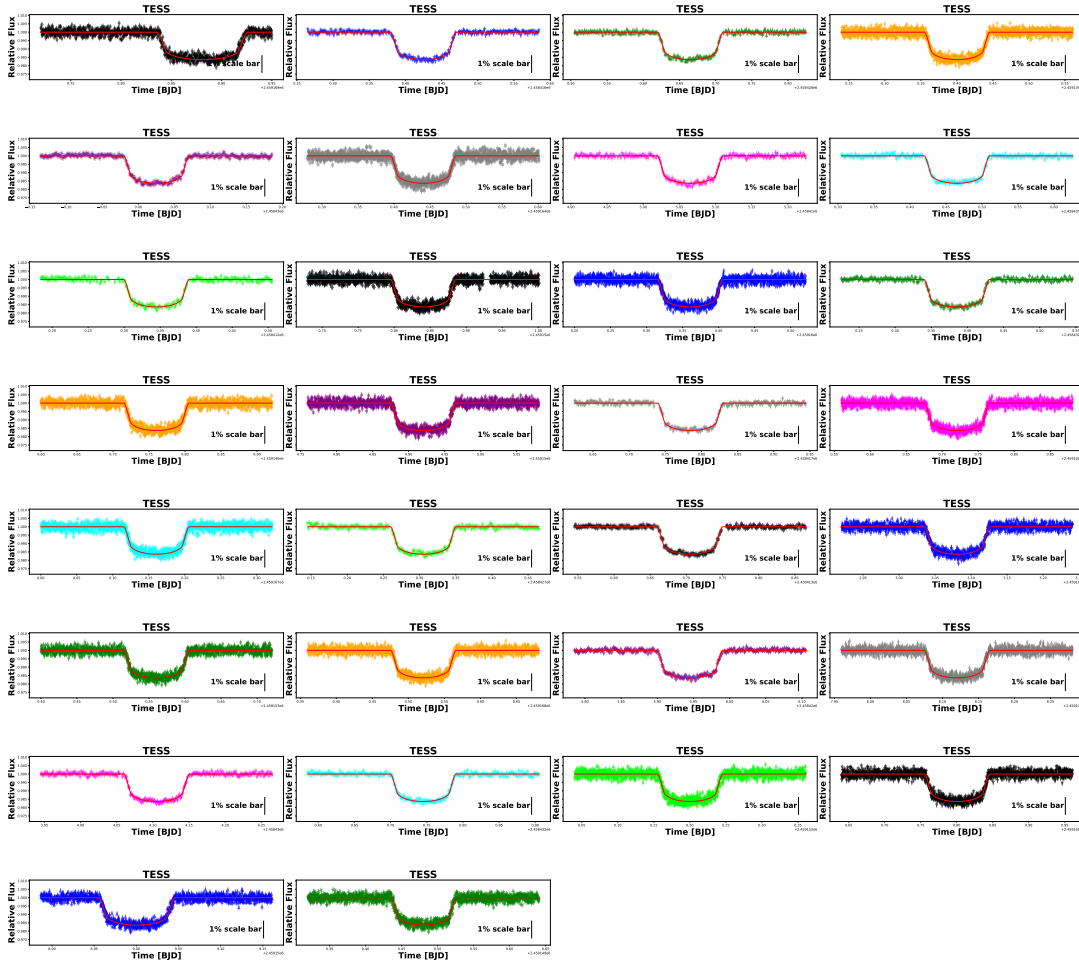


Figure 2. These individual light curves are produced from the 30 TESS transit observations during the process described in [Transit Photometry Reduction](#) Section 4.1. The wellness of fit in each light curve demonstrates the reliability of TESS for precise transit photometry measurements. TESS observations span approximately 2 years from October, 2018 to November, 2020.

3.3. Eclipse Data

The derivation of accurate and precise eclipse ephemerides is also critical for the efficient use of space-based observatory time (e.g., [Zellem et al. 2020](#); [Pearson et al. 2022](#); [Burt et al. 2024, in prep](#)). We used six mid-eclipse times to derive the mid-eclipse ephemeris for this study (Table 5). Eclipse data for WASP-77 A b came from JWST NIRSpec (Program GTO 1274 [August et al. 2023](#)) with NRS1 and NRS2 covering the wavelength ranges of $2.674 - 3.716 \mu\text{m}$ and $3.827 - 5.173 \mu\text{m}$, respectively. We utilized eclipse light curves from HST/WFC3+G141 grism between 1.1 and $1.7 \mu\text{m}$ (Program GO-16168 [Mansfield et al. 2022](#)). Two of the six mid-eclipse times were estimated from publicly-available phase curves obtained by the Spitzer Space Telescope ([Werner et al. 2004](#)) IRAC2 ([Fazio et al. 2004](#)) at 3.6 and $4.5 \mu\text{m}$ (Program GO-13038). For more information about the analyses of the eclipse data, see [Eclipse Data Reduction](#) Section 4.2. Two additional mid-eclipse times were taken directly from Spitzer (Program GO-10102) and derived by [Garhart et al. \(2020\)](#).

Table 5. Mid-Eclipse Times Used In This Study

Source	Mid-eclipse (BJDTDB)	Mid-eclipse Uncertainty (days)
JWST (this study)	2459816.57496	0.00013
HST (this study)	2459161.04312	0.0003
Spitzer IRAC2 3.6 μ m (this study)	2457854.05090	0.00043
Spitzer IRAC2 4.5 μ m (this study)	2457722.12849	0.00041
Spitzer IRAC2 3.6 μ m Garhart et al. (2020)	2456975.47418	0.00070
Spitzer IRAC2 4.5 μ m Garhart et al. (2020)	2456978.19514	0.00076

NOTE—This table lists the six mid-eclipse times that were used in joint fit analysis in [Joint Simultaneous Fit of Transit, Eclipse, and Radial Velocity Data](#) Section 4.5.

3.4. Radial Velocity Data

We considered radial velocity observations from five public sources, ultimately selecting three for inclusion in the final analysis. Two data sets came from the WASP-77 A b discovery paper ([Maxted et al. 2013](#), Table 6). The first (Program 088.C-0011(A)), from the HARPS spectrograph on the 3.6-meter telescope at the European Southern Observatory’s (ESO) La Silla Observatory in Chile ([Mayor et al. 2003](#)). The second was from CORALIE, a high-resolution radial velocity spectrograph which is attached to the 1.2-meter telescope at La Silla ([Queloz et al. 2000](#)). We also included a set of HARPS radial velocities (Program 0102.C-0618(A)) taken after the instrument’s fiber upgrade in 2015. These post-upgrade HARPS data (hereafter referred to as HARPS15) are obtained from the December 11, 2023 ESO/HARPS Radial Velocities Catalog ([Barbieri 2023](#)) see Table 7).

We identified an additional set of radial velocity observations taken with the SOPHIE spectrograph, located at the Haute-Provence Observatory in southern France ([Bouchy et al. 2009](#)). The SOPHIE data could not be confirmed by the SOPHIE team as having passed requisite quality checks, thus, these data were excluded from our analysis. We also identified data taken with ESO’s radial velocity spectrograph, ESPRESSO ([Pepe et al. 2021](#)), but noted that this data was taken during the planet’s transit as part of a Rossiter-McLaughlin ([Rossiter 1924](#); [McLaughlin 1924](#)) analysis, and thus did not include these data in our analysis. To accurately detect the influence of WASP-77 A b on the host star’s orbital velocity, individual points taken during Rossiter-McLaughlin effect were excluded which can contain shifts in the measured radial velocity. One radial velocity measurement was removed from CORALIE and eight from HARPS15 that were taken during transit. Our final data set for analysis included 8 radial velocity measurements from HARPS, 10 from CORALIE, and 14 from HARPS15.

Table 6. WASP-77 A b Archival Radial Velocity Measurements from HARPS and CORALIE Spectrographs from Discovery

Instrument	BJDTDB	RV (m/s)	RV uncertainty (m/s)
HARPS	2455832.8615	1462.6	2.0
HARPS	2455832.9040	1511.1	2.4
HARPS	2455832.9110	1523.3	2.5
HARPS	2455889.7458	1406.3	3.6
HARPS	2455890.5370	2022.0	3.7
HARPS	2455890.7386	1865.6	4.1
HARPS	2455891.5721	1767.0	4.4
HARPS	2455891.7468	1988.5	4.6
CORALIE	2455069.7803	1324.6	4.9
CORALIE	2455163.6091	1336.2	5.2
CORALIE	2455169.6920	1967.3	4.9
CORALIE	2455170.6625	1570.6	5.3
CORALIE	2455188.6258	1969.6	5.4
CORALIE	2455856.7095	1865.5	5.3
CORALIE	2455914.6783	1710.5	4.3
CORALIE	2455915.6775	1332.8	4.4
CORALIE	2455916.6681	1708.7	4.8
CORALIE	2455917.6500	1954.4	4.7
CORALIE	2455918.6645	1554.2	6.5

NOTE—The table contains the radial velocity (RV) data from the discovery paper (Maxted et al. 2013) used in the radial velocity analysis as described in [Radial Velocity Analysis](#) Section 4.4. Radial velocity measurement from 2455916.6681 BJD TDB is removed from analysis as it was taken during transit with Rossiter-McLaughlin effect.

Table 7. WASP-77 A b Archival Radial Velocity Measurements from HARPS Post 2015 Spectrograph Upgrade

Instrument	BJDTBD	RV (m/s)	RV uncertainty (m/s)
HARPS15	2458427.787554	1470.018000	1.573475
HARPS15	2458428.560896	1879.973206	1.785650
HARPS15	2458428.570433	1868.396660	2.194125
HARPS15	2458428.582250	1851.242091	2.868588
HARPS15	2458428.593025	1831.094489	2.098265
HARPS15	2458428.603905	1817.661492	2.013355
HARPS15	2458428.614680	1806.211830	1.762600
HARPS15	2458428.625664	1807.350545	1.740453
HARPS15	2458428.636231	1812.432497	1.752132
HARPS15	2458428.646902	1783.755312	1.610181
HARPS15	2458428.657677	1750.562875	1.630013
HARPS15	2458428.668452	1713.482612	1.643702
HARPS15	2458428.679135	1680.066842	1.828763
HARPS15	2458428.690003	1649.613223	1.723875
HARPS15	2458428.700778	1647.376523	1.634059
HARPS15	2458428.711762	1653.280585	1.612155
HARPS15	2458428.722444	1638.297547	1.559323
HARPS15	2458428.733219	1624.977366	1.527627
HARPS15	2458428.743891	1608.904283	1.506273
HARPS15	2458428.754562	1595.072828	1.538156
HARPS15	2458428.765441	1578.391821	1.595225
HARPS15	2458428.776216	1.568452064	1.563796

NOTE—Radial velocity (RV) data from the December 11, 2023 ESO/HARPS Radial Velocities Catalog ((Barbieri 2023) used in this study. Eight measurements taken during the planets transit that were affected by Rositter-Mclaughlin effect, are removed from analysis for measurements between 2458428.63 and 2458428.71 BJDTDB. The remaining 14 radial velocity observations listed here are fit as described in Radial Velocity Analysis Section 4.4.

4. ANALYSIS

Using these transit photometry, eclipse photometry and radial velocity data, we performed a joint orbital analysis for WASP 77 A b. Our methodology adheres to the process described in Pearson et al. (2022).

4.1. Transit Photometry Reduction

We modeled individual light curves for each photometric time series to derive the best-fit parameters including transit depth, inclination, and mid-transit time. We performed model fitting of transit light curves using EXOTIC (EXOplanet Transit Interpretation Code), a comprehensive Python data reduction tool designed to support the citizen science and professional community in analyzing exoplanet transit data (Zellem et al. 2020; Fatahi 2024, in prep). The code uses priors from the NASA Exoplanet Archive, ensuring the use of the most-recently published system parameters. EXOTIC yields full posteriors and uncertainties for each parameter.

To enhance the precision of our parameter estimates, we employed UltraNest (Buchner 2016), a robust multimodal nested sampling algorithm. To prevent the influence of data points that might not represent significant transit signals, light curves with residuals larger than the transit depth were removed to ensure that the model’s fit captured significant transit signals from WASP-77 A b. Individual data points failing a 3σ clip were discarded prior to fitting the light curve. Observations with a flux standard deviation greater than 0.03 were also excluded to eliminate data with excessive noise, as high scatter can indicate instability in the observations or environmental contamination. Observations with airmass values larger than 2 were excluded.

Table 8. Stellar Priors Used for This Study

Parameter	Units	(Cortés-Zuleta et al. 2020)
M_*	mass [M_\odot]	$0.903 \pm 6.6 \times 10^{-2}$
R_*	radius [R_\odot]	$0.910 \pm 2.5 \times 10^{-2}$
T_{eff}	Effective temperature [K]	$5617 \pm 7.2 \times 10^1$
Metallicity (dex)	[Fe/H]	$-0.10 \pm 1.1 \times 10^{-1}$
Stellar surface gravity	$\log g$ ($\log_{10}(\text{cm/s}^2)$)	$4.476 \pm 1.5 \times 10^{-2}$

For ExoClock and ETD observations that did not include airmass or the elevation of the observatory, we calculated the airmass values by extracting the latitude and longitude of the observer’s location and then used the Google Maps API to derive the elevation based on geographic data. This geographic information was then passed to EXOTIC to calculate the airmass values for each time stamp of the corresponding observation.

Limb darkening coefficients depend on the host stellar parameters and the wavelength at which the observation was taken and must be derived to fit the model accurately. Based on the filter used for the observations, we assigned a corresponding passband within EXOTIC utilizing the Python package **Exotethys** (Morello et al. 2020) with stellar parameters for effective temperature $5617 \pm 7.2 \times 10^1$ kelvin, Metallicity (dex) $-0.10 \pm 1.1 \times 10^{-1}$ [Fe/H], and stellar surface gravity $4.476 \pm 1.5 \times 10^{-2} \log g$ ($\log_{10}(\text{cm/s}^2)$) (Cortés-Zuleta et al. 2020) (see Table 8) to derive the limb darkening coefficients for each fit.

The citizen science mid-transit times and TESS data were incorporated into a comprehensive joint transit, eclipse and radial velocity analysis described in [Joint Simultaneous Fit of Transit, Eclipse, and Radial Velocity Data](#) Section 4.5. (Refer to Tables 1, 2, 3 and 4 for the list of mid-transit times from Exoplanet Watch, ExoClock, ETD, and TESS.) Properly model fitting the individual transit data accounting for airmass and limb darkening effects provided constraints on the transits’ inclination, RpRs, and most relevant to our study, precise mid-transit times for our joint transit, eclipse and radial velocity analysis. The resulting citizen science individual mid-transit times were used as priors in our joint fit analysis in 4.5.

4.2. Eclipse Data Reduction

The two JWST eclipse light curves from August et al. (2023) were simultaneously fit together here to derive one mid-eclipse time via the same global fit process used for the transit data in [Global Fits of Citizen Science and TESS Transit Data for Comparison](#) Section 4.3. The same process is used for two HST eclipse light curves from Mansfield et al. (2022). The Spitzer eclipse data were processed using a public pipeline based on the pixel-map method (Lewis et al. 2013) with additional optimizations for handling the ramp effect and uncertainty estimation using nested sampling. The pipeline uses gaussian kernel regression with a nearest neighbor technique to estimate the intrapixel sensitivities in each dataset. Non-physical solutions can arise if the priors are too large and not correlated to one another with consequences manifesting as negative night-side temperatures and wildly varying hot-spot offsets compared to GCM models. To avoid non-physical solutions, we used conditional priors to model the phase curve components (i.e., day-night amplitude and hot-spot offset) which is important for deriving physically-plausible solutions when using a linear system of equations. Two additional Spitzer mid-eclipse (emid) values were adopted from Garhart et al. (2020).

4.3. Global Fits of Citizen Science and TESS Transit Data for Comparison

The lightcurves individually fit for better constraints on transit parameters described in [Transit Photometry Reduction](#) Section 4.1, were combined and fit simultaneously here in a global fit in order to compare the use of citizen science and professional transit data sets. The inclination, planet-to-star radius ratio, and the mid-transit time were left as free parameters in the individual fits and, once derived, were passed to the global fit for more precise constraints on these parameters with the addition of the

orbital period. For the global fit, in order to ensure the ephemeris remains fresh longer, we adopted the mid-transit time from the most recent available light curve in the corresponding data set as our weighted prior for the new ephemeris. See [Results and Discussion Section 5](#) for results and comparison of the global fits.

4.4. Radial Velocity Analysis

To determine if stellar variability impacted in the HARPS and CORALIE data, we searched for correlations between various activity indicators and the radial velocity data ([Saar & Donahue 1997](#); [Desort et al. 2007](#); [Lovis & Fischer 2011](#)). Specifically, we made use of two spectral line indicators (H-alpha and the S-index) and three metrics from the radial velocity Cross Correlation Functions (CCF), the FWHM, BIS, and Contrast. These values provide insights on whether the magnetic phenomena exhibited by a star, such as spots, plages, and granulation, are impacting the stellar absorption lines significantly enough to impact the measured radial velocities.

After the individual indices were calculated, we measured their Pearson correlation coefficients with the radial velocity data. The highest-ranked index was the FWHM, which had a correlation coefficient of 0.58 with the radial velocities. As this was below the $r = 0.6$ limit generally used to identify moderate correlation ([Akoglu 2018](#)), we asserted that WASP-77 A exhibits no significant stellar activity, and therefore we did not include activity-mitigation steps in our radial velocity fitting methodology. Radial velocity measurements spanning the full orbital phase of an exoplanet are crucial for determining accurate system parameters ([Cumming et al. 1999](#); [Ford 2005](#); [Hara et al. 2017](#)). In particular, the shape of the orbit cannot usually be constrained by transit photometry alone ([Kipping 2008](#)). By including radial velocities throughout the planet's orbit in our analysis [Fig. 3](#), we can determine the eccentricity of WASP-77 A b's orbit accurately ([Cumming et al. 1999](#); [Wright & Howard 2009](#)). We adopted the [Pearson et al. \(2022\)](#) methodology of using a Keplerian model to fit the radial velocity data and determine the orbital period, argument of periastron, eccentricity, and semi-amplitude of WASP-77 A b.

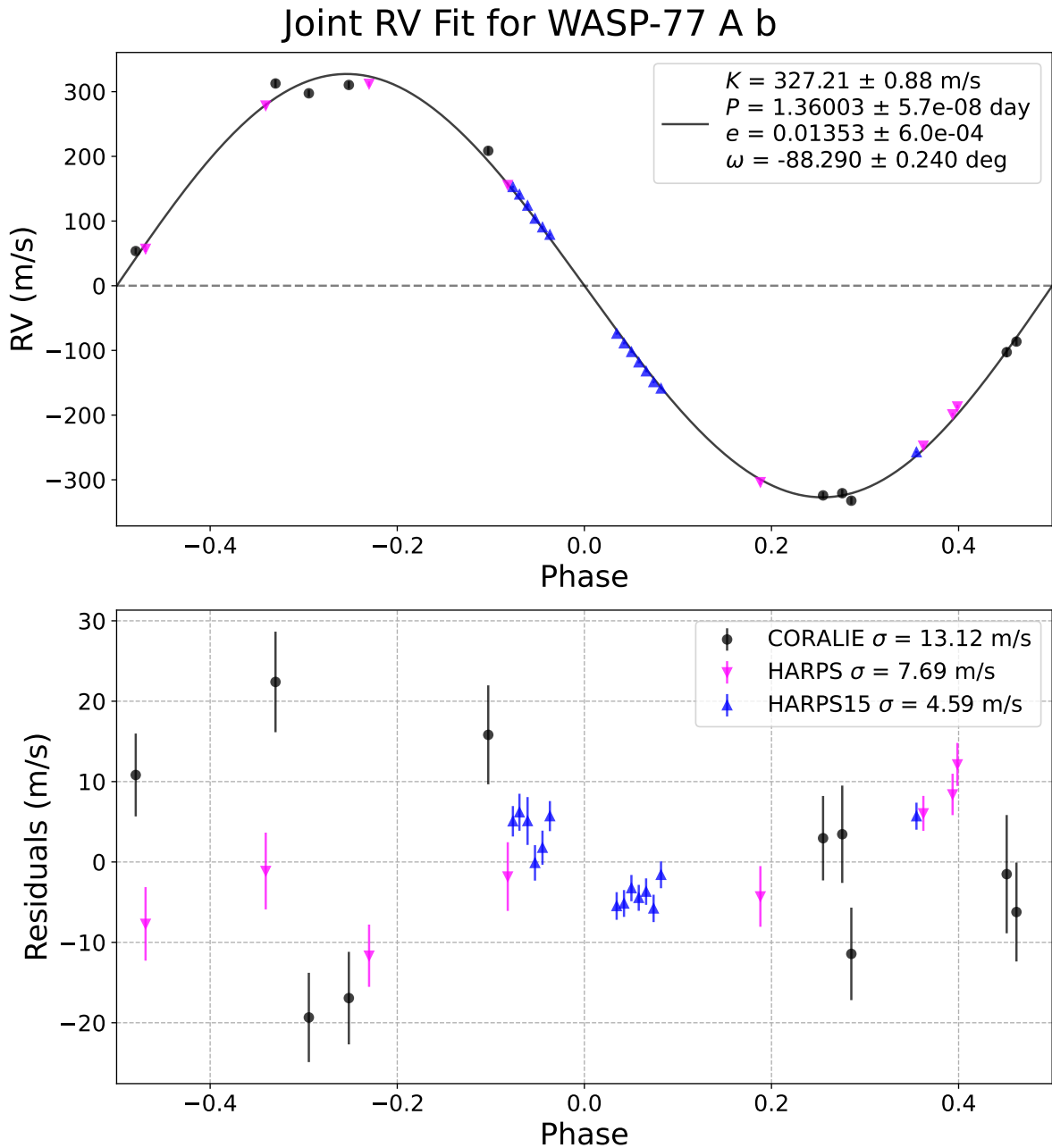


Figure 3. Top: phase-folded radial velocity curve for WASP-77 A b. The radial velocity data included are from the discovery paper [Maxted et al. \(2013\)](#) and recent HARPS data from the ESO archive. Bottom: radial velocity residuals for WASP-77 A b after removing the contribution for the planetary orbit.

4.5. Joint Simultaneous Fit of Transit, Eclipse, and Radial Velocity Data

We leveraged a joint-simultaneous fit of the transit, eclipse, and radial velocity data to place strong constraints on the system parameters, including new transit and eclipse ephemerides, following the prescription of [Pearson et al. \(2022\)](#). To do so, we coupled the underlying orbit equations between the planet and star to ensure a self consistent solution — something that is not possible when using separate code-bases for each respective measurement type. We updated WASP-77 A b’s parameters for orbital period, mid-transit time, inclination, argument of periastron, eccentricity, planet mass, and the radius ratio between the planet and the star with a nested sampler. Our joint analysis utilized the

stellar priors in Table 8 from Cortés-Zuleta et al. (2020). The joint optimization leveraged a combined likelihood function with contributions from radial velocity, photometry, and ephemerides: $L_{joint} = L_{RV} + L_{transit} + L_{mid-transit} + L_{mid-eclipse}$.

The final posterior distributions from the nested sampling algorithm can be seen in Figure 4 depicting the most probable parameter estimates and their uncertainties. The Gaussian distribution about the narrow likelihood maximum peak ensures we effectively explore the parameter space and that our estimates represent the data.

The stacked light curves in Figure 5 from TESS, display the wellness of fit when analyzed simultaneously with eclipse and radial velocity data in the joint analysis. The TESS stacked lightcurves yield a 856σ detection of the transit depth $R_p/R_*^2 = 0.013695 \pm 1.6 \times 10^{-5}$. Mid-transit times for the citizen science data were incorporated into the joint fit as priors. For individual fit plots of the transit data, see Figures 1 and 2. Table 9 presents our joint fit final parameters with comparison to prior work described in Results and Discussion Section 5. The observed minus calculated (O-C) diagram presented in Figure 6 illustrates the mid-eclipse timing residuals for WASP-77 A b from our joint analysis. The grey error bars represent a 1σ uncertainty from the predicted mid-eclipse time. We also produce an O-C plot for WASP-77 A b's mid-transit times (Fig. 7) which indicates how much our ephemeris derived here (grey-shaded region) improves upon the current ephemeris uncertainty in the published literature (Cortés-Zuleta et al. 2020) (pink shaded region).

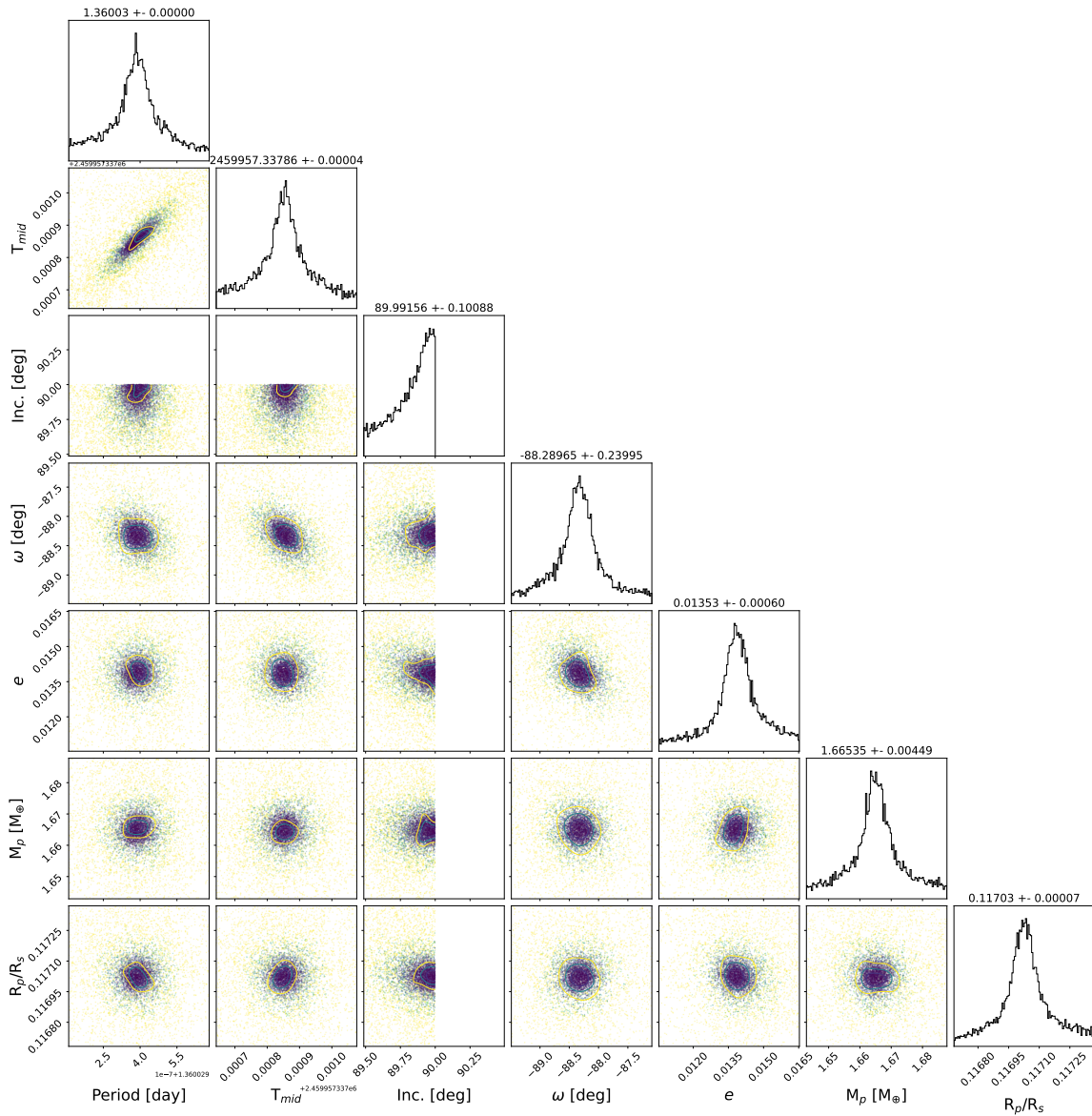


Figure 4. Posterior plot depicting the most probable parameter estimates and their uncertainties from our joint transit, eclipse and radial velocity data fit for period, mid-transit time, inclination, argument of periastron, eccentricity, mass of planet, and planet star radius ratio. The contour plots indicate the density of the probability distribution with the inner contour representing a 1 sigma deviation. The shape and orientation of the contour plots are indicative of the amount of correlation between parameters with a more circular shape depicting less correlation. The narrow peaks in the figure represent the most probable estimates with a Gaussian distribution illustrating uncertainties for fit parameters. In the case of inclination, we deliberately restrict the upper limit to 90° to reflect the physical limitation on this parameter; consequently, the cone is truncated on right side for inclination.

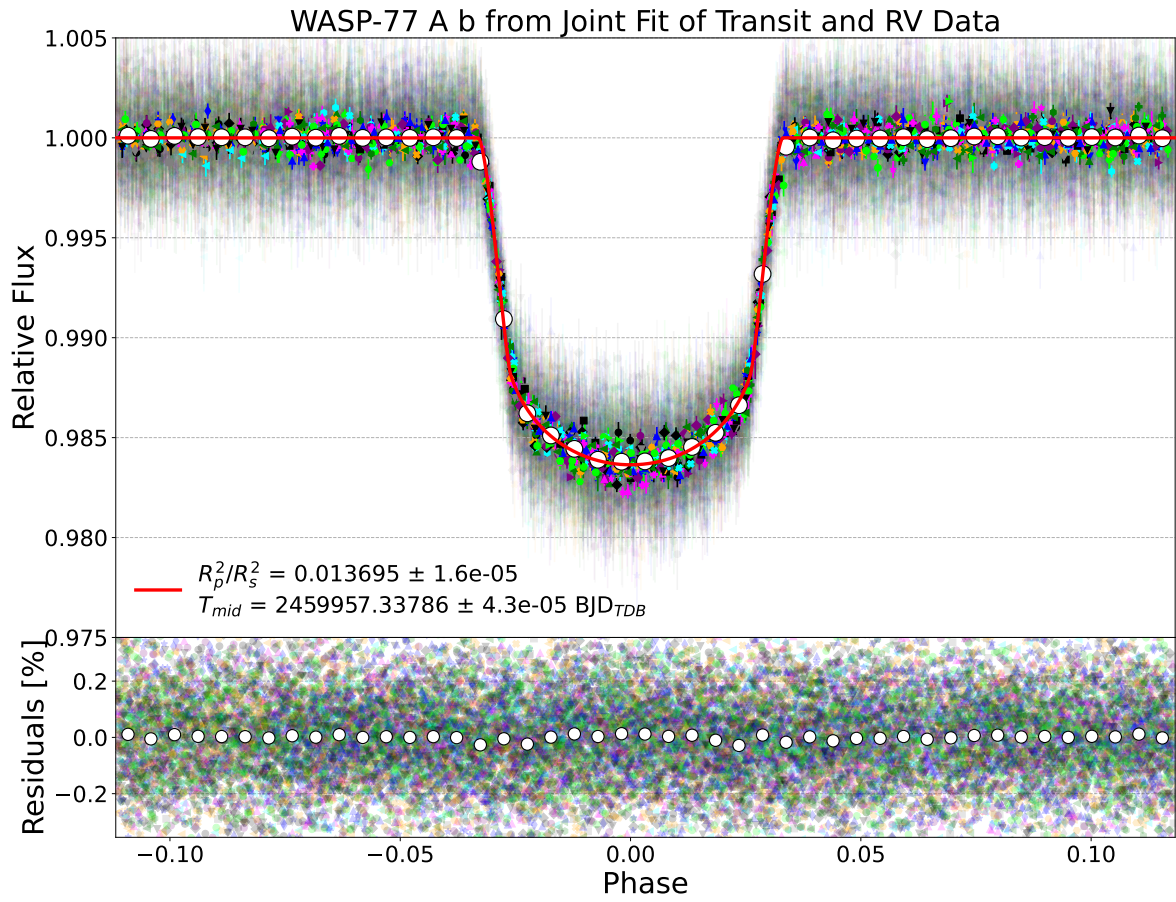


Figure 5. We present the phase-folded TESS transit data from the joint simultaneous fit of WASP-77 A b. The top plot is a stacked light curve plot from *Joint Simultaneous Fit of Transit, Eclipse, and Radial Velocity Data* Section 4.5 depicting the wellness of fit. The transit data is displayed as colored points, with the predicted light curve displayed as a red line. The lower plot is the residuals illustrating the difference between the observation data and the model.

Table 9. System Parameters for WASP-77 A b Joint Fit Comparison with Prior Papers

Parameter	Units	(Cortés-Zuleta et al. 2020)	(Kokori et al. 2023)	This Work
P	Orbital Period [days]	$1.36002854 \pm 6.2 \times 10^{-7}$	$1.360028949 \pm 7.5 \times 10^{-8}$	$1.360029395 \pm 5.7 \times 10^{-8}$
T_{mid}	Mid-transit time [BJDTDB]	$2457420.88439 \pm 8.5 \times 10^{-4}$	$2458693.870688 \pm 3.9 \times 10^{-5}$	$2459957.337860 \pm 4.3 \times 10^{-5}$
E_{mid}	Mid-Eclipse time [BJDTDB]	$2457658.2054 \pm 4.4 \times 10^{-3}$	<i>n/a</i>	$2459956.658192 \pm 6.7 \times 10^{-5}$
i	Inclination [deg]	$88.91 \pm 9.5 \times 10^{-1}$	<i>n/a</i>	$89.99 \pm 1.0 \times 10^{-1}$
ω	Argument of periastron [deg]	$-166 \pm 7.5 \times 10^{+1}$	<i>n/a</i>	$-88.29 \pm 2.4 \times 10^{-1}$
e	Eccentricity	$0.00740 \pm 6.9 \times 10^{-3}$	<i>n/a</i>	$0.01353 \pm 6.0 \times 10^{-4}$
M_p	Mass of planet [M_{Jup}]	$1.667 \pm 6.8 \times 10^{-2}$	<i>n/a</i>	$1.6654 \pm 4.5 \times 10^{-3}$
R_p/R_*	Radius of planet in stellar radii	$0.13354 \pm 7.4 \times 10^{-4}$	<i>n/a</i>	$0.117026 \pm 6.9 \times 10^{-5}$
a	Semi-major axis [AU]	$0.02335 \pm 4.5 \times 10^{-4}$	<i>n/a</i>	$0.023233633 \pm 3.7 \times 10^{-8}$
a/R_*	Semi-major axis in stellar radii	$5.332 \pm 8.1 \times 10^{-2}$	<i>n/a</i>	$5.4900859 \pm 8.6 \times 10^{-6}$
K	Radial Velocity semi-amplitude [m/s]	$323.4 \pm 3.8 \times 10^0$	<i>n/a</i>	$327.21 \pm 8.8 \times 10^{-1}$
Propagated T_{mid} to 2030-01-01	[BJDTDB]	$2462503.31104 \pm 2.47 \times 10^{-3}$ (± 213 sec)	$2462503.311774 \pm 2.14 \times 10^{-4}$ (± 18 sec)	$2462503.312887 \pm 1.15 \times 10^{-4}$ (± 9.9 sec)
Propagated E_{mid} to 2030-01-01	[BJDTDB]	$2462502.6271 \pm 4.9 \times 10^{-3}$ (± 425.35 sec)	<i>n/a</i>	$2462502.633219 \pm 1.26 \times 10^{-4}$ (± 10.89 sec)

NOTE—This table cross-references the parameters in the joint transit, eclipse, and radial velocity fit to prior publications on WASP-77 A b: (Cortés-Zuleta et al. 2020; Kokori et al. 2023).

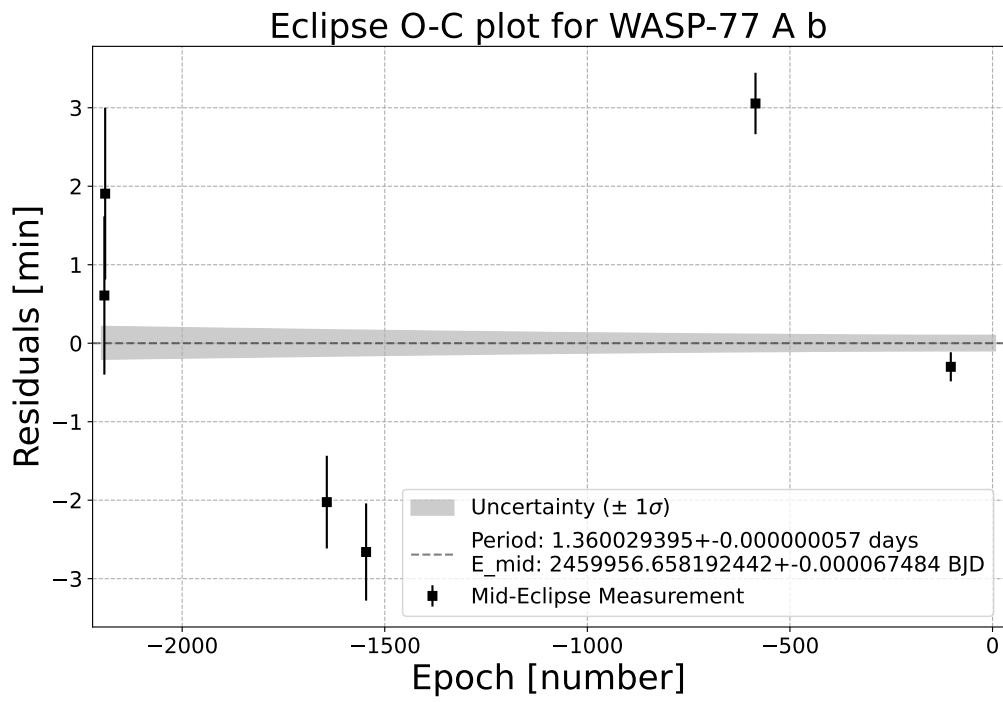


Figure 6. Eclipse O-C plot for WASP-77 A b with mid-eclipse times as listed in Table 5. The residuals are shown in minutes and represent the difference between the observed and calculated mid-eclipse times based on a fixed linear ephemeris. The grey bar denotes a 1σ uncertainty. This constricted grey region illustrates the power of our analysis in ensuring a fresh eclipse ephemeris.

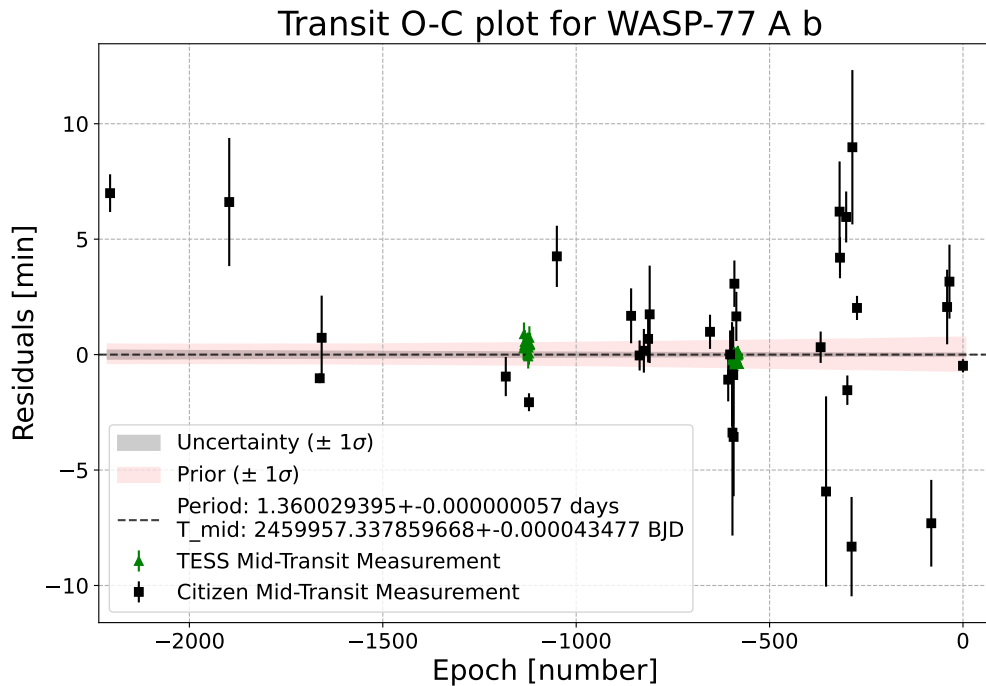


Figure 7. O-C plot for mid-transit times of WASP-77 A b based on our joint analysis. The residuals are shown in minutes and represent the difference between the observed and calculated mid-transit times based on a fixed linear ephemeris. The grey bar denotes a 1σ uncertainty. The pink shaded area indicates the propagated uncertainty of the prior ephemeris without incorporating the updates from our current study. The distribution of residuals around the zero line validates the precision of the updated orbital parameters.

4.6. Transit Timing Variation Analysis

Transit timing variations (TTVs), periodic perturbations to the mid-transit times of a known planet, can indicate the presence of additional planets in a system (e.g., Agol et al. 2005; Holman & Murray 2005; Ford et al. 2012; Hadden & Lithwick 2016; Pearson 2019). TTVs can reveal long-term periodic trends, usually associated with precession, as well as short-order perturbations (Ragozzine & Holman 2010; Deck 2014; Pearson 2019; Korth 2020), so a two-term model is needed to capture the dynamics of both. We generated Lomb-Scargle periodograms to look for Transit Timing Variations (TTVs) in the O-C data residuals, indicating potential periodic signals in the power versus orbital period, Figure 8.

For our WASP-77 A b data, we calculated BIC values for a linear fit and a Fourier fit to the data to help us determine which model better represents the data. If there is periodicity in the mid-transit times, then the Fourier fit will have the lower BIC value as it can detect periodicity that cannot be detected by the linear model (Schwarz 1978). When comparing Bayesian Information Criterion (BIC) values between different models, the model with the lowest BIC is typically considered the best fit to the data (Schwarz 1978) and is derived by the equation:

$$BIC = k \ln(n) - 2 \ln(\hat{L}), \quad (1)$$

where k is the number of parameters estimated by the model, n is the number of observations or sample size, and \hat{L} is the maximized value of the likelihood function of the model. The term $k \cdot \ln(n)$ penalizes complexity to avoid overfitting, while $-2 \cdot \ln(\hat{L})$ pertains to the goodness of fit.

The false alarm probability (FAP) is a statistical measure used to assess the likelihood that a perceived signal in the data could arise from random fluctuations alone rather than any actual periodic variation (Xie et al. 2014). FAP values are ultimately used, along with Bayesian evidence, to signify the presence or absence of a periodic variation in our transit times.

Panel A describes the power versus orbital period. Panel B overplots the O-C data with our two Fourier models, while Panels C and D depict phase-folded solutions for Fourier fit 1 and 2 respectively,

illustrating how well they correspond with the observed data. In the phase folded plots, the x-axis is in phase relative to orbital epochs determined by the mid-transit point of the orbit and period, indicating that the mid-transit times are plotted against the phase of the planet's orbit. Each point represents the deviation of the observed transit time from a predicted time, based on the orbital period. Based on the BIC values, we do not find a significant periodic trend with a single term. We do not see significant evidence for a two-term periodic model and report no transit timing variations in the mid-transit times from this study.

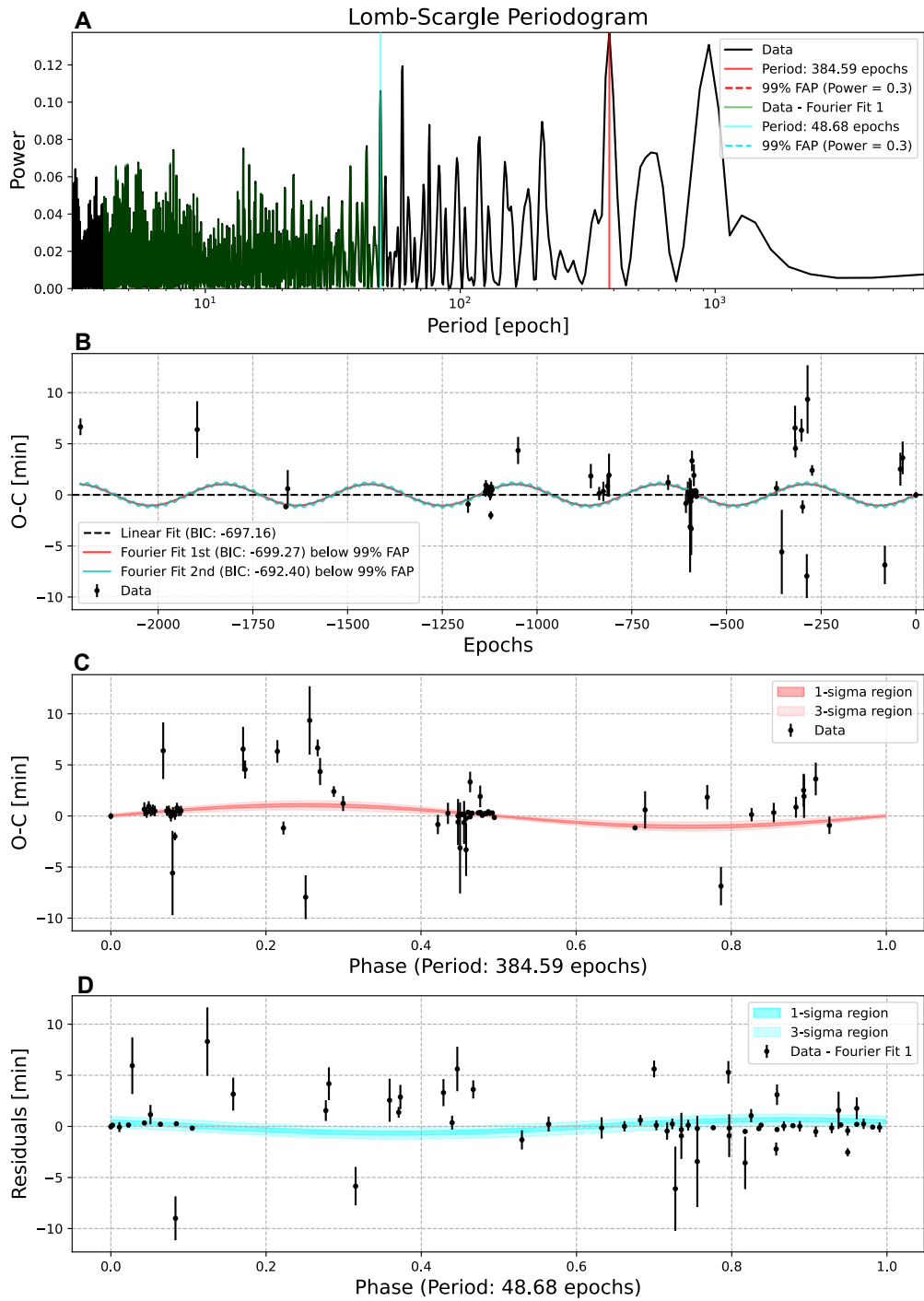


Figure 8. Diagnostic plots to search for transit timing variations using a periodogram analysis with the Lomb-Scargle algorithm. A) Power versus orbital period plot indicating the potential for underlying periodic signals. “Detrended” data also presented. B) O-C data overlaid with single-period (Fourier Fit 1) and two-period (Fourier Fit 2) models. C) A phase-folded solution for Fourier fit 1. Based on the BIC value reported in B, we do not find a significant periodic trend with a single term. D) A phase-folded plot for the second term in Fourier fit 2 after subtracting the first term. For more details, please see TTV Analysis [Transit Timing Variation Analysis Section 4.6](#).

5. RESULTS AND DISCUSSION

Our joint analysis of the combined radial velocity, eclipse, and transit data set, constrains the orbital parameters of WASP 77 A b to high precision (Table 9). We present a new orbital period of $1.360029395 \pm 5.7 \times 10^{-8}$ days, mid-transit time of $2459957.337860 \pm 4.3 \times 10^{-5}$ BJD_{TDB}, mid-eclipse time of $2459956.658192 \pm 6.7 \times 10^{-5}$ BJD_{TDB}, inclination $89.99 \pm 1.0 \times 10^{-1}$ [deg], argument of periastron $-88.29 \pm 2.4 \times 10^{-1}$ [deg], eccentricity $0.01353 \pm 6.0 \times 10^{-4}$, mass of planet $1.6654 \pm 4.5 \times 10^{-3} M_{Jup}$, radius of planet in stellar radii $0.117026 \pm 6.9 \times 10^{-5} R_p/R_*$, semi-major axis $0.023233633 \pm 3.7 \times 10^{-8}$ [AU], semi-major axis in stellar radii $5.4900859 \pm 8.6 \times 10^{-6} a/R_*$, and radial Velocity semi-amplitude $327.21 \pm 8.8 \times 10^{-1} K$ [m/s].

5.1. Forward Propagation of Transit and Eclipse

To accurately predict future transit and eclipse times and their uncertainties for WASP-77 A b, we employed an analytical error propagation method for forward propagation using the notation of [Zellem et al. \(2020\)](#). The precise prediction of an exoplanet’s next transit time (T_{mid}) is given through the equation:

$$T_{\text{mid}} = n_{\text{orbit}} \cdot P + T_0 \quad (2)$$

where n_{orbit} represents the number of orbits until the future transit event, P is the orbital period of the planet, and T_0 is the established mid-transit or mid-eclipse time. The analytical derivation of the uncertainty in the mid-transit time (ΔT_{mid}) incorporates the propagation of errors in the orbital period (ΔP) and the starting mid-transit time (ΔT_0), as:

$$\Delta T_{\text{mid}} = \sqrt{(n_{\text{orbit}}^2) \cdot (\Delta P^2) + (\Delta T_0^2)}. \quad (3)$$

The prior mid-transit time we constrained and propagated was taken from the most recent transit data which was from an Exoplanet Watch user. Using the most recent observation reduces the uncertainties that older published mid-transit times may have.

For our joint fit analysis results of the citizen science and TESS transit data, eclipse data, and radial velocity data, we find a January 1, 2030 (a reasonable date for the start of the Ariel mission science operations ([Burt et al. 2024, in prep](#))) propagated mid-transit uncertainty of ± 9.94 seconds. Similarly, from the joint fit analysis we find a propagated mid-eclipse time uncertainty of ± 10.89 seconds. Our forward-propagation results demonstrate how we can obtain a lower uncertainty in the propagated mid-transit time with the addition of all of the latest available data. Compared to a previously published mid-transit time from a similar study by [Cortés-Zuleta et al. \(2020\)](#), we demonstrate we can achieve a tighter constraint on the forward propagated mid-transit time by a factor of 21.5 by including the latest data. When our new mid-eclipse time is forward propagated to January 1, 2030, we improve precision by a factor of 39.1 compared to the previous study’s propagated mid-eclipse time ([Cortés-Zuleta et al. 2020](#)).

We also compared forward propagated mid-transit times from the global fits of the citizen science data alone, the TESS data alone, and then with these two combined sources, to quantify the benefit of incorporating citizen science data when updating exoplanet ephemerides. The resulting mid-transit times and errors were also forward propagated to the date January 1, 2030. The TESS data alone produces a mid-transit time uncertainty on January 1, 2030 of ± 40.35 seconds, while the citizen science data alone produces a propagated mid-transit time uncertainty of ± 22.55 seconds (Table 10). The lower uncertainty, despite the larger per-measurement uncertainty, may be due to a longer time baseline of the citizen science data giving an advantage in constraining some parameters like period and mid-transit time. The longer baseline may explain why the derived parameters have smaller uncertainties in the citizen science data alone fit, by enabling us to effectively bin down the noise and constrain the ephemeris more precisely than with the TESS data. We can compensate for the lower SNR measurements with more measurements over a longer baseline ([Dragomir et al. 2020](#)). While this is a minimal difference in the observational padding required, it nonetheless demonstrates how the broader baseline of the citizen science observations increases the mid-transit time precision beyond what is possible with the higher precision, but more temporally concentrated, TESS data alone. Figure 7 depicts the concentrated TESS data and temporal spread of the citizen science data illustrating how these observations can aid in filling in gaps between TESS sectors. Unsurprisingly, our global fit analysis demonstrates that we obtain the

Table 10. Parameters for comparison of global fits and joint transit + eclipse + RV analysis.

Parameter	Units	Citizen Science	TESS	Citizen Science+TESS	Transit+Eclipse+RV
P	[days]	1.36002984 $\pm 1.2 \times 10^{-7}$	1.36002877 $\pm 1.9 \times 10^{-7}$	1.36002947 $\pm 1.0 \times 10^{-7}$	1.360029395 $\pm 5.7 \times 10^{-8}$
T_{mid}	[BJDTDB]	2459957.33826 $\pm 1.3 \times 10^{-4}$	2459169.880764 $\pm 3.5 \times 10^{-5}$	2459957.337881 $\pm 7.4 \times 10^{-5}$	2459957.337860 $\pm 4.3 \times 10^{-5}$
	[degree]	90.00 $\pm 1.1 \times 10^{-1}$	88.073 $\pm 5.3 \times 10^{-2}$	88.371 $\pm 5.9 \times 10^{-2}$	89.99 $\pm 1.0 \times 10^{-1}$
R_p/R_*	[ratio]	0.11500 $\pm 2.8 \times 10^{-4}$	0.11746 $\pm 1.1 \times 10^{-4}$	0.117012 $\pm 9.7 \times 10^{-5}$	0.117026 $\pm 6.9 \times 10^{-5}$
Transit light curves	#	34	30	64	64 transit, 6 eclipse
Radial velocity measurements	#	<i>n/a</i>	<i>n/a</i>	<i>n/a</i>	32
Propagated Mid-Transit to Jan 1 2030	[BJDTDB]	2462503.31412 $\pm 2.61 \times 10^{-4}$ ($\pm 22.55sec$)	2462503.311279 $\pm 4.67 \times 10^{-4}$ ($\pm 40.35sec$)	2462503.313049 $\pm 2.01 \times 10^{-4}$ ($\pm 17.37sec$)	2462503.312887 $\pm 1.26 \times 10^{-4}$ ($\pm 9.94sec$)

NOTE—This table cross-references the ephemerides between the fits of only the terrestrial citizen science transit data, only TESS transit data, combined citizen science with TESS data, and the final joint fitting, which included both citizen science and TESS transit data with eclipse and radial velocity data.

most precise constraints when we combine both the citizen science and TESS photometry data, which produces a January 1, 2030 mid-transit time uncertainty of ± 17.37 seconds, a factor of 2.3 improvement over the TESS data alone.

The stacked TESS and citizen science light curves (Figure 9) show excellent agreement with the best-fit model. We can infer from the quality of the fit that the model is reliably fitting the citizen science and TESS data to derive the parameters of WASP-77 A b. The low uncertainty on transit depth of $0.013692 \pm 2.3 \times 10^{-5}$ and the random distribution about 0 in the residuals implies a good fit between the data and the model. The ephemeris improvement with the addition of citizen science data further demonstrates the importance of utilizing all available data in conjunction with the continuous yield of TESS to fill in the gaps and keep exoplanet ephemerides fresh.

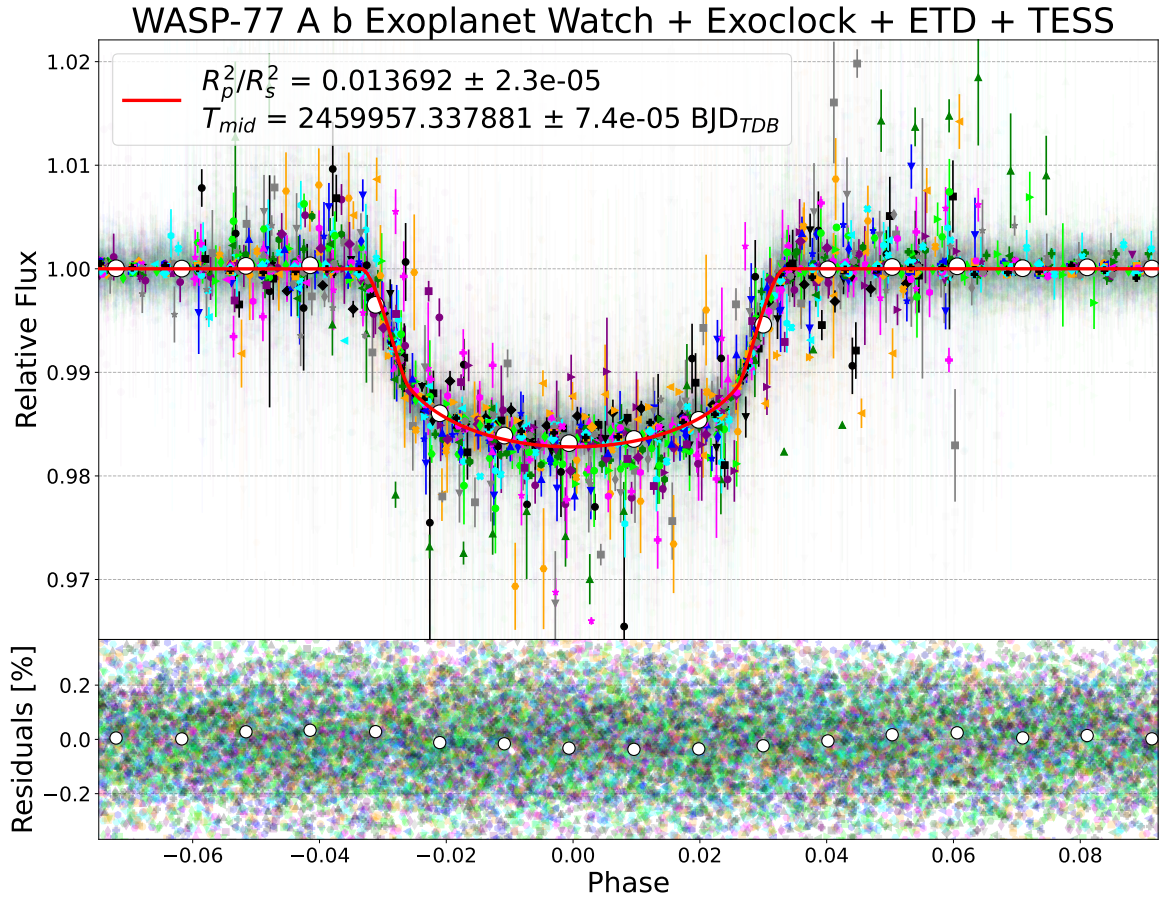


Figure 9. The top plot is a stacked light curve plot from global fit analysis described in [Global Fits of Citizen Science and TESS Transit Data for Comparison](#) Section 4.3 and 5.1 of WASP-77 A b. The lower plots are the residuals depicting the difference between the observation data and the model. For individual fit plots of the transit data, please see Figures 1 and 2.

6. CONCLUSION

A cornerstone of this effort is the joint-simultaneous analysis of transit photometry, eclipse photometry, and radial velocity measurements. By merging these data types, we are able to achieve a high level of precision in the best-fit model for WASP-77 A b with a new orbital period improved to $1.360029395 \pm 5.7 \times 10^{-8}$ days, mid-transit time to $2459957.337860 \pm 4.3 \times 10^{-5}$ BJD_{TDB}, mid-eclipse time to $2459956.658192 \pm 6.7 \times 10^{-5}$ BJD_{TDB} and mass to $1.6654 \pm 4.5 \times 10^{-3} M_J$. Methodology from this study aids the community in updating exoplanet ephemerides precisely and showcasing the impact of collaborative data use and nested sampling ([Pearson et al. 2022](#)).

The code for this study will be made publicly available on GitHub so that professional and citizen scientists can precisely update ephemerides of targets scheduled for observations by JWST and Ariel. With new innovations in obtaining spectroscopic measurements such as EXCITE (Exoplanet Climate Infrared Telescope) ([Bernard et al. 2022](#); [Tucker et al. 2018](#)) or the Pandora SmallSat ([Quintana et al. 2021](#); [Hoffman et al. 2022](#)), along with existing technologies, this code can be used by scientists for planning observations and performing atmospheric models that require the most precise and up to date ephemerides.

The incorporation of citizen science data from sources such as Exoplanet Watch, Exoclock, and ETD in our study was an integral component of the achieved precision in the updating of WASP-77 A b’s ephemeris giving us a broader time baseline. Furthermore, our results demonstrate that when citizen

science light curve data is added to the TESS data it improves the propagated January 1, 2030 mid-transit time uncertainty by a factor of 2.3. By incorporating citizen science observations into this study, we were able to leverage an observation taken on January 12, 2023 that would have not be possible without planned observations with space-based and large ground-based telescopes or by using previously published mid-transit times alone. With the number of newly discovered exoplanets continuing to grow there is an ongoing need for continued ephemeris maintenance. Dragomir et al. (2020) demonstrates that exoplanets observed by TESS can have an over 30 minute uncertainty on the mid-transit time only one year after it was observed. By supporting citizen science-based exoplanet initiatives, the astronomy community can keep up with the demand for exoplanet ephemeris updates.

Our study underscores the significant impact of combining various data sources by including citizen science contributions, ground-based observations, space telescope data, and radial velocity measurements, for the refinement of exoplanetary parameters. This comprehensive approach not only enhances the precision of orbital parameters crucial for atmospheric characterization but also improves the observation scheduling for missions like JWST and Ariel. The application of our publicly available Python code can be applied to various exoplanets, fitting radial velocity, transit, and eclipse data from both professional and citizen science sources substantially increasing ephemeris precision for the community. We advocate for sustained support of citizen science data contributions.

Software: EXOTIC (Zellem et al. 2020), WOTAN (Hippke et al. 2019), Exotethys (Morello et al. 2020), UltraNest (Buchner 2016)

7. ACKNOWLEDGEMENTS

Some of the research described in this publication was carried out in part at the Jet Propulsion Laboratory, California Institute of Technology, under a contract with the National Aeronautics and Space Administration.

This research has used the NASA Exoplanet Archive and ExoFOP, which is operated by the California Institute of Technology, under contract with the National Aeronautics and Space Administration under the Exoplanet Exploration Program.

This publication uses data products from Exoplanet Watch, a citizen science project managed by NASA’s Jet Propulsion Laboratory on behalf of NASA’s Universe of Learning.

This work is supported by NASA under award number NNX16AC65A to the Space Telescope Science Institute, in partnership with Caltech/IPAC, Center for Astrophysics—Harvard & Smithsonian, and NASA Jet Propulsion Laboratory.

This research has used the NASA/IPAC Infrared Science Archive, which is funded by the National Aeronautics and Space Administration and operated by the California Institute of Technology.

This work is based in part on observations made with the Spitzer Space Telescope, which was operated by the Jet Propulsion Laboratory, California Institute of Technology, under a contract with NASA. NASA provided support for this work through an award issued by JPL/Caltech.

Based on observations collected at the European Southern Observatory under ESO programs 088.C-0011(A) and 1102.C-0744(C).

We thank the Ronald Greeley Planetary Scholarship at Arizona State University for supporting Suber Corley for this work.

The authors extend their gratitude to the Data and Analysis Center for Exoplanets (DACE) team at the University of Geneva. As we embarked on this journey into exoplanet research utilizing radial velocity, their DACE Python package, online graphical tool, and accompanying tutorials proved invaluable in helping us grasp the nuances of radial velocity data analysis. We particularly appreciate their prompt and unwavering support when we reached out for assistance. Their willingness to share expertise and enrich the broader community is exemplary and we are truly thankful for that.

This research has made use of NASA’s Astrophysics Data System. Some/all of the data presented in this paper were obtained from the Mikulski Archive for Space Telescopes (MAST). STScI is operated by the Association of Universities for Research in Astronomy, Inc., under NASA contract NAS5-26555. Support for MAST for non-HST data is provided by the NASA Office of Space Science via grant NNX13AC07G and by other grants and contracts.

Some/all of the data presented in this paper were obtained from the Mikulski Archive for Space Telescopes (MAST) at the Space Telescope Science Institute. The specific observations analyzed can be accessed via [doi:10.17909/t9-nmc8-f686](https://doi.org/10.17909/t9-nmc8-f686), [doi:10.17909/T97P46](https://doi.org/10.17909/T97P46), [doi:10.17909/3fmp-zj55](https://doi.org/10.17909/3fmp-zj55).

STScI is operated by the Association of Universities for Research in Astronomy, Inc., under NASA contract NAS5-26555. Support to MAST for these data is provided by the NASA Office of Space Science via grant NAG5-7584 and by other grants and contracts.

This research has made use of the SIMBAD database, operated at CDS, Strasbourg, France.

We acknowledge with thanks the transit observations from the AAVSO International Database contributed by observers worldwide and used in this research.

This research has made use of the VizieR catalogue access tool, CDS, Strasbourg, France.

Observation taken by Jake Postiglione was funded by PSC-CUNY Award 65172-00 53

Based on observations collected at the European Organisation for Astronomical Research in the Southern Hemisphere under ESO programme(s) 088.C-0011(A), and 0102.C-0618(A).

Based on data obtained from the ESO Science Archive Facility with DOI(s): <https://doi.org/10.18727/archive/33>

MicroObservatory is maintained and operated as an educational service by the Center for Astrophysics Harvard and Smithsonian and is a project of NASA's Universe of Learning, supported by NASA Award NNX16AC65A. Additional MicroObservatory sponsors include the National Science Foundation, NASA, the Arthur Vining Davis Foundations, Harvard University, and the Smithsonian Institution.

We thank Frank Sienkiewicz of the Science Education department, CfA, who maintains and schedules the MicroObservatory telescopes for exoplanet observations.

P. S. acknowledges support provided by NASA through the NASA FINESST grant 80NSSC22K1598.

REFERENCES

- Agol, E., Steffen, J., Sari, R., & Clarkson, W. 2005, *Monthly Notices of the Royal Astronomical Society*, 359, 567
- Akoglu, H. 2018, *Turkish journal of emergency medicine*, 18, 91
- August, P. C., Bean, J. L., Zhang, M., et al. 2023, *arXiv e-prints*, arXiv:2305.07753, doi: [10.48550/arXiv.2305.07753](https://doi.org/10.48550/arXiv.2305.07753)
- Barbieri, M. 2023, *arXiv e-prints*, arXiv:2312.06586, doi: [10.48550/arXiv.2312.06586](https://doi.org/10.48550/arXiv.2312.06586)
- Batalha, N. E., Lewis, N. K., Line, M. R., Valenti, J., & Stevenson, K. 2018, *ApJL*, 856, L34, doi: [10.3847/2041-8213/aab896](https://doi.org/10.3847/2041-8213/aab896)
- Bernard, L., Jensen, L., Gamaunt, J., et al. 2022, in *Ground-based and Airborne Instrumentation for Astronomy IX*, Vol. 12184, SPIE, 763–772
- Bitsch, B., Schneider, A. D., & Kreidberg, L. 2022, *arXiv preprint arXiv:2207.06077*
- Bouchy, F., Hébrard, G., Udry, S., et al. 2009, *A&A*, 505, 853, doi: [10.1051/0004-6361/200912427](https://doi.org/10.1051/0004-6361/200912427)
- Buchner, J. 2016, *Statistics and Computing*, 26, 383, doi: [10.1007/s11222-014-9512-y](https://doi.org/10.1007/s11222-014-9512-y)
- Burt, J., Zellem, R., Ciardi, D., et al. 2024, in prep, *AJ*
- Cortés-Zuleta, P., Rojo, P., Wang, S., et al. 2020, *Astronomy & Astrophysics*, 636, A98
- Cumming, A., Marcy, G. W., & Butler, R. P. 1999, *The Astrophysical Journal*, 526, 890
- Deck, K. M. 2014, PhD thesis, Massachusetts Institute of Technology
- Desort, M., Lagrange, A.-M., Galland, F., Udry, S., & Mayor, M. 2007, *Astronomy & Astrophysics*, 473, 983
- Dragomir, D., Kempton, E., Bean, J., et al. 2019, *BAAS*, 51, 422, doi: [10.48550/arXiv.1903.09173](https://doi.org/10.48550/arXiv.1903.09173)
- Dragomir, D., Harris, M., Pepper, J., et al. 2020, *AJ*, 159, 219, doi: [10.3847/1538-3881/ab845d](https://doi.org/10.3847/1538-3881/ab845d)
- Eastman, J., Siverd, R., & Gaudi, B. S. 2010, *PASP*, 122, 935, doi: [10.1086/655938](https://doi.org/10.1086/655938)
- Edwards, B., & Changeat, Q. 2024, *The Astrophysical Journal Letters*, 962, L30
- Fatahi, T. 2024, in prep
- Fazio, G., Hora, J., Allen, L., et al. 2004, *The Astrophysical Journal Supplement Series*, 154, 10
- Ford, E. B. 2005, *The Astronomical Journal*, 129, 1706
- Ford, E. B., Ragozzine, D., Rowe, J. F., et al. 2012, *The Astrophysical Journal*, 756, 185
- Fowler, M. J. F., Sienkiewicz, F. F., Zellem, R. T., & Dussault, M. E. 2021, *Journal of the British Astronomical Association*, 131, 359, doi: [10.48550/arXiv.2007.13381](https://doi.org/10.48550/arXiv.2007.13381)

- Garhart, E., Deming, D., Mandell, A., et al. 2020, *The Astronomical Journal*, 159, 137
- Hadden, S., & Lithwick, Y. 2016, *The Astrophysical Journal*, 828, 44
- Hara, N. C., Boué, G., Laskar, J., & Correia, A. 2017, *Monthly Notices of the Royal Astronomical Society*, 464, 1220
- Hewitt, H. B., Simon, M. N., Mead, C., et al. 2023b, *Physical Review Physics Education Research*, 19, 020156
- Hewitt, H. B., Noguier, F., Corley, S., et al. 2023, *JAAVSO*, 51, 6.
<https://app.aavso.org/jaavso/article/3876/>
- Hippke, M., David, T. J., Mulders, G. D., & Heller, R. 2019, *AJ*, 158, 143,
doi: [10.3847/1538-3881/ab3984](https://doi.org/10.3847/1538-3881/ab3984)
- Hoffman, K., Quintana, E. V., Dotson, J. L., et al. 2022, in *Space Telescopes and Instrumentation 2022: Optical, Infrared, and Millimeter Wave*, Vol. 12180, SPIE, 80–88
- Holman, M. J., & Murray, N. W. 2005, *Science*, 307, 1288
- Hord, B. J., Kempton, E. M.-R., Mikal-Evans, T., et al. 2023, arXiv preprint arXiv:2308.09617
- Kempton, E. M.-R., Bean, J. L., Louie, D. R., et al. 2018, *Publications of the Astronomical Society of the Pacific*, 130, 114401
- Khorshid, N., Min, M., & Désert, J. 2023, *Astronomy & Astrophysics*, 675, A95
- Kipping, D. M. 2008, *Monthly Notices of the Royal Astronomical Society*, 389, 1383
- Kokori, A. 2021, in *European Planetary Science Congress, EPSC2021–650*,
doi: [10.5194/epsc2021-650](https://doi.org/10.5194/epsc2021-650)
- Kokori, A., Tsiaras, A., Edwards, B., et al. 2022a, *Experimental Astronomy*, 53, 547
- . 2022b, *The Astrophysical Journal Supplement Series*, 258, 40
- Kokori, A., Tsiaras, A., Edwards, B., et al. 2023, *ApJS*, 265, 4, doi: [10.3847/1538-4365/ac9da4](https://doi.org/10.3847/1538-4365/ac9da4)
- Kokori, A., Tsiaras, A., Edwards, B., et al. 2023, *The Astrophysical Journal Supplement Series*, 265, 4
- Korth, J. 2020, PhD thesis, Universität zu Köln
- Kunimoto, M., Winn, J., Ricker, G. R., & Vanderspek, R. K. 2022, *AJ*, 163, 290,
doi: [10.3847/1538-3881/ac68e3](https://doi.org/10.3847/1538-3881/ac68e3)
- Lewis, N. K., Knutson, H. A., Showman, A. P., et al. 2013, *ApJ*, 766, 95,
doi: [10.1088/0004-637X/766/2/95](https://doi.org/10.1088/0004-637X/766/2/95)
- Line, M. R., Brogi, M., Bean, J. L., et al. 2021, *Nature*, 598, 580
- Lovis, C., & Fischer, D. 2011, *Exoplanets*, edited by S. Seager. Tucson, AZ: University of Arizona Press, 2011, 526 pp. ISBN 978-0-8165-2945-2., p.27-53
- Madhusudhan, N., Bitsch, B., Johansen, A., & Eriksson, L. 2017, *Monthly Notices of the Royal Astronomical Society*, 469, 4102
- Mansfield, M., Wisner, L., Stevenson, K. B., et al. 2022, *The Astronomical Journal*, 163, 261,
doi: [10.3847/1538-3881/ac658f](https://doi.org/10.3847/1538-3881/ac658f)
- Maxted, P. F. L., Anderson, D. R., Collier Cameron, A., et al. 2013, *PASP*, 125, 48,
doi: [10.1086/669231](https://doi.org/10.1086/669231)
- Mayor, M., Pepe, F., Queloz, D., et al. 2003, *The Messenger*, 114, 20
- McLaughlin, D. 1924, *Astrophysical Journal*, 60, 22-31 (1924), 60
- Mizrachi, R., Ly, D., Bewersdorff, L., & Tock, K. 2021, *Journal of the American Association of Variable Star Observers (JAAVSO)*, 49, 186
- Morello, G., Claret, A., Martin-Lagarde, M., et al. 2020, *AJ*, 159, 75, doi: [10.3847/1538-3881/ab63dc](https://doi.org/10.3847/1538-3881/ab63dc)
- Pearson, K. A. 2019, *AJ*, 158, 243,
doi: [10.3847/1538-3881/ab4e1c](https://doi.org/10.3847/1538-3881/ab4e1c)
- Pearson, K. A., Beichman, C., Fulton, B. J., et al. 2022, *AJ*, 164, 178,
doi: [10.3847/1538-3881/ac8dee](https://doi.org/10.3847/1538-3881/ac8dee)
- Peluso, D. O., Esposito, T. M., Marchis, F., et al. 2023, *Publications of the Astronomical Society of the Pacific*, 135, 015001
- Pepe, F., Cristiani, S., Rebolo, R., et al. 2021, *A&A*, 645, A96, doi: [10.1051/0004-6361/202038306](https://doi.org/10.1051/0004-6361/202038306)
- Poddaný, S., Brát, L., & Pejcha, O. 2010, *NewA*, 15, 297, doi: [10.1016/j.newast.2009.09.001](https://doi.org/10.1016/j.newast.2009.09.001)
- Queloz, D., Mayor, M., Naef, D., et al. 2000, in *From Extrasolar Planets to Cosmology: The VLT Opening Symposium*, ed. J. Bergeron & A. Renzini, 548, doi: [10.1007/10720961_79](https://doi.org/10.1007/10720961_79)
- Quintana, E. V., Colón, K. D., Mosby, G., et al. 2021, arXiv preprint arXiv:2108.06438
- Ragozzine, D., & Holman, M. J. 2010, arXiv preprint arXiv:1006.3727
- Ricker, G. R., Winn, J. N., Vanderspek, R., et al. 2015, *Journal of Astronomical Telescopes, Instruments, and Systems*, 1, 014003
- Rossiter, R. 1924, *Astrophysical Journal*, 60, 15-21 (1924), 60
- Saar, S. H., & Donahue, R. A. 1997, *The Astrophysical Journal*, 485, 319

- Sadler, P. M., Gould, R. R., Leiker, P. S., et al. 2001, *Journal of Science Education and Technology*, 10, 39
- Schwarz, G. 1978, *The annals of statistics*, 461
- Smith, P. C., Line, M. R., Bean, J. L., et al. 2024, *The Astronomical Journal*, 167, 110
- Tucker, G. S., Nagler, P., Butler, N., et al. 2018, in *Ground-based and Airborne Instrumentation for Astronomy VII*, Vol. 10702, International Society for Optics and Photonics, 107025G, doi: [10.1117/12.2314225](https://doi.org/10.1117/12.2314225)
- Werner, M. W., Roellig, T. L., Low, F. J., et al. 2004, *ApJS*, 154, 1, doi: [10.1086/422992](https://doi.org/10.1086/422992)
- Wright, J., & Howard, A. 2009, *The Astrophysical Journal Supplement Series*, 182, 205
- Xie, J.-W., Wu, Y., & Lithwick, Y. 2014, *The Astrophysical Journal*, 789, 165
- Zellem, R. T., Swain, M. R., Roudier, G., et al. 2017, *The Astrophysical Journal*, 844, 27
- Zellem, R. T., Pearson, K. A., Blaser, E., et al. 2020, *PASP*, 132, 054401, doi: [10.1088/1538-3873/ab7ee7](https://doi.org/10.1088/1538-3873/ab7ee7)